



Article

Adaptive Backstepping Nonsingular Terminal Sliding-Mode Attitude Control of Flexible Airships with Actuator Faults

Shiqian Liu ^{1,*}, James F. Whidborne ², Sipeng Song ³ and Weizhi Lyu ¹

¹ School of Aeronautics and Astronautics, Shanghai Jiao Tong University, Shanghai 200240, China; weizhi_lyu@sjtu.edu.cn

² School of Aerospace, Transport and Manufacturing, Cranfield University, Cranfield MK43 0AL, UK; j.f.whidborne@cranfield.ac.uk

³ AVIC Xi'an Flight Automatic Control Research Institute, Xi'an 710065, China; nwpussp@163.com

* Correspondence: liushiqian@sjtu.edu.cn; Tel.: +86-21-3420-7967

Abstract: This paper studies the attitude tracking control of a flexible airship subjected to wind disturbances, actuator saturation and control surface faults. Efficient flexible airship models, including elastic deformation, rigid body motions, and their coupling, are established via Lagrange theory. A fast-nonsingular terminal sliding-mode (NTSM) combined with a backstepping control is proposed for the problem. The benefits of this approach are NTSM merits of high robustness, fast transient response, and finite time convergence, as well as the backstepping control in terms of globally asymptotic stability. However, the major limitation of the backstepping NTSM is that its design procedure is dependent on the prior knowledge of the bound values of the disturbance and faults. To overcome this limitation, a wind observer is designed to compensate for the effect of the wind disturbances, an anti-windup compensator is designed to compensate for actuator saturation, and an adaptive fault estimator is designed to estimate the faults of the control surfaces. Globally exponential stability of the closed-loop control system is guaranteed by using the Lyapunov stability theory. Finally, simulation results demonstrate effectiveness and advantages of the proposed control for the Skyship-500 flexible airship, even in the presence of unknown wind disturbances, control surface faults, and different stiffness variants.

Keywords: flexible airship; fast-nonsingular terminal sliding-mode control; backstepping control; wind disturbance observer; fault tolerant control



Citation: Liu, S.; Whidborne, J.F.; Song, S.; Lyu, W. Adaptive Backstepping Nonsingular Terminal Sliding-Mode Attitude Control of Flexible Airships with Actuator Faults. *Aerospace* **2022**, *9*, 209. <https://doi.org/10.3390/aerospace9040209>

Academic Editors: Carlo E. D. Riboldi and Norman M. Wereley

Received: 27 December 2021

Accepted: 15 March 2022

Published: 11 April 2022

Publisher's Note: MDPI stays neutral with regard to jurisdictional claims in published maps and institutional affiliations.



Copyright: © 2022 by the authors. Licensee MDPI, Basel, Switzerland. This article is an open access article distributed under the terms and conditions of the Creative Commons Attribution (CC BY) license (<https://creativecommons.org/licenses/by/4.0/>).

1. Introduction

Airships have many potential applications for transport, environment surveillance, communication relay, and aerial photography, etc. These applications have attracted much research interest [1]. As one of the lighter-than-air unmanned vehicles, reliable autonomous control is highly desired for different airship missions. Thus, the key objective is to realize accurate trajectory-tracking control for the unmanned airship. However, due to the inherent system nonlinearity and underactuation of the airship under diverse environment disturbances, this makes the trajectory-tracking control of the airship quite challenging and difficult.

To achieve high-precision tracking performance, many control schemes of the airship have been proposed to solve the trajectory tracking problem, which includes gain scheduling control [2], backstepping design [3,4], sliding-mode control [5,6], neural network control [7,8], and fuzzy control [9]. Among these methods, the sliding-mode control and backstepping design are potentially useful approaches to overcome disturbance and faults of the airship. The backstepping approach has been proposed for the robust control of nonlinear systems in a strict feedback form through the construction of control Lyapunov functions (CLFs) [10]. The nonlinear backstepping design has been widely studied for various aerospace and underwater vehicle control problems [11,12]. Meanwhile,

the sliding-mode control, due to its insensitivity to disturbances and model uncertainties, has been applied to the trajectory-tracking control for the airship with unknown disturbances and winds [5]. To make the output response quickly converge to the desired values, the terminal sliding-mode control (SMC) is proposed for robust control within a finite time [7,13]. Mofid et al. proposed a super-twisting terminal SMC and barrier function terminal SMC to deal with the quad-rotor unmanned aerial vehicles (UAVs) with delay input [14] and drive the error dynamics to converge on a region near the origin within a finite time [15]. The event-triggered fractional-order SMC technique was proposed to stabilize the quadrotor UAV with external random/time-varying disturbances [16]. In addition, recently, some researchers developed the backstepping sliding-mode control design to use combination merits of SMC and the backstepping design [17,18].

On the other hand, the system faults and disturbances of the airship are unknown and nonlinear. Thus, it is necessary for disturbance rejection and fault compensation to achieve the desired robust performance. Guo et al. [19] investigated a distributed fault-tolerant sliding-mode control for 2-D plane vehicular platoon systems, where a neuro-adaptive fault-tolerant control scheme was implemented by combining a sliding-mode control technique with a radial basis function neural network (RBFNN) to guarantee the finite-time stability. Xiao et al. [20] proposed an adaptive integral sliding-mode approach to realize fault-tolerant tracking control for a multi-vectored thrust ellipsoidal airship. Liu and Whidborne [8] proposed a neural network adaptive backstepping fault tolerant control for the unmanned airship with multi-vectored thrusters. These methods not only guarantee the system with faults of robust stability, but also tolerate the unknown actuator faults, even in the disturbance environment.

However, all the above nonlinear designs are focused on rigid-body airship models, which cannot guarantee the performance for flexible cases. To realize high altitude and long endurance missions, the stratospheric airship often uses the flexible inflated membrane material as the airship hull; thus, the weight is lighter and endurance is longer. Unlike conventional rigid airships, the mutual interaction between flexibility, aerodynamics, and flight dynamics of flexible airships should be modeled [21,22], because this interaction will improve the model precision and control performance [23]. For the trajectory-tracking control of the flexible airship, Li et al. [21] proposed an integrated model, including the flight dynamics, structural dynamics, aerostatics, and aerodynamics, but they only analyzed the linear mode characteristics of the flexible airship without consideration of nonlinear control problems. The main difficulties for the flexible airship are nonlinear and coupling control between the rigid and flexible body. Bennaceur and Azouz [24] proposed a Lagrangian method to build up an efficient model of flexible airships. In addition, Han et al. [25] proposed a command filtered backstepping approach to design the trajectory controller for a flexible airship. However, they did not consider disturbances and fault effects on the flexible airship, both of which can result in system instability. In fact, from long endurance-hovering in the air and working in diverse environments day and night, the sensors and actuators of the flexible stratospheric airship are easily impaired. Thus, fault tolerant control of the airship with actuator faults is studied here.

Motivated by Li's [21] and Han's work [25], the main work in this paper is a novel backstepping nonsingular terminal sliding-mode (BNTSM) control scheme proposed for attitude tracking of the airship with unknown faults, disturbances, and actuator saturation. In the proposed BNTSM control scheme, the nonsingular terminal sliding-mode technique and backstepping technique are integrated. The proposed BNTSM control has advantages of high robustness, fast transient response, and finite time convergence, and the globally asymptotic stability of the closed-loop system can be guaranteed. Furthermore, a wind observer and an adaptive fault estimator are designed to observe the wind disturbances and estimate the control surface faults; thus, the limitation of the BNTSM control dependent on prior knowledge is overcome. The main contributions of the proposed scheme are summarized as follows.

1. A backstepping nonsingular terminal sliding-mode control scheme is proposed for attitude tracking control of the flexible airship with actuator faults, actuator saturation, and uncertainties of stiffness.
2. A wind observer with an adaptive disturbance observer is designed to reject variable external bounded disturbances and cope with model parameter uncertainties.
3. An anti-windup compensator based on proportion to saturation errors is used to compensate actuator saturation.
4. An adaptive fault estimator is incorporated into the BNTSM control to implement fault estimation and fault tolerant control.

This paper is organized as follows. The nonlinear dynamics-modeling of the flexible airship and the robust control problem are described in Section 2. The BNTSM control is proposed in Section 3, and stability is proven for the corresponding closed-loop tracking system. In Section 4, three scenarios are simulated to demonstrate the BNTSM control performance. Section 5 gives the conclusions.

2. Airship Modeling and Problem Formulation

The structure of the flexible airship is shown in Figure 1. There are four control surfaces, including two rudders and two elevators on the tail fins, and two propellers are set up on each side of the hull. The gondola under the airship envelope houses the avionics system and the flight control system and other payloads.

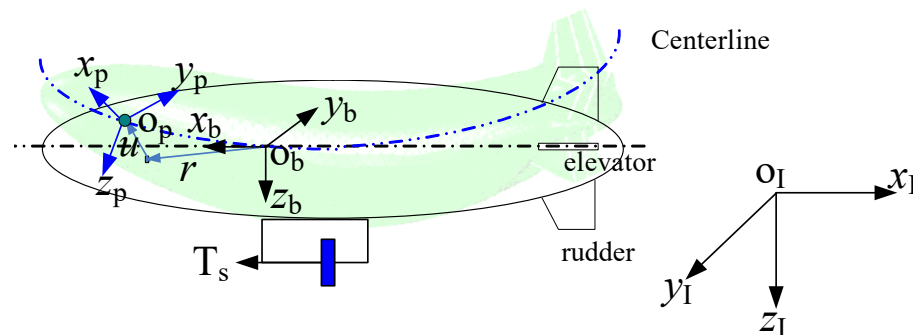


Figure 1. Structure of the flexible airship and the reference frames.

2.1. Airship Kinematics Model

The equations of motion of a flexible airship are expressed in a body frame $F_b\{O_b x_b y_b z_b\}$ fixed on the undeformed airship with its origin, O_b , at the center of volume (CV), see Figure 1. The motion of the airship is described as the translation and rotation of this body frame with respect to the inertial frame $F_I\{O_I x_I y_I z_I\}$, plus the deformation of the material points on the body relative to the body frame [21]. A centerline frame $F_p\{O_p x_p y_p z_p\}$ is introduced to calculate the aerodynamics forces of the flexible airship. The elastic displacement u of a material point on the airship can be written by a summation of the shape functions, as

$$u = \sum q_i(t) \Phi_i(r), \quad (i = 1, 2, \dots, N) \tag{1}$$

where q_i are the time-dependent generalized coordinates, $\Phi_i = [\Phi_{xi} \ \Phi_{yi} \ \Phi_{zi}]^T$ are the structural mode shape vector, and r is the position vector of the material point from the origin, O_b . The associated velocity distribution over the elastic body is:

$$v = v_a + \Omega \times r + \Omega \times u + \dot{u} \tag{2}$$

where $v_a = [u, v, w]^T$ is the translational velocity vector in F_b , $\Omega = [p \ q \ r]^T$ is the angular rate vector, and the \times denotes cross-product operation. The first two terms of Equation (2) are related to the rigid body translation and rotation, while the last two terms reflect the influence of the elasticity on the local velocity.

Assume the airship is modeled as a free-free Euler–Bernoulli beam only undergoing bending deformation; hence, if the internal pressure is high enough to prevent wrinkling, then the hull bending can be described as the fundamental mode shape of the airship. The shape functions Φ are chosen as the natural vibration mode shapes of the beam, and $2N$ shape functions are employed to describe the airship’s deflection, that is,

$$\begin{cases} \Phi_i = [0 \ \Phi_i \ 0]^T, \text{ the bending in the Oxy plane} \\ \Phi_{N+i} = [0 \ 0 \ \Phi_i]^T, \text{ the bending in the Oxz plane} \end{cases} \quad (i = 1, 2, \dots, N) \quad (3)$$

where Φ_i is the i th natural mode shape of the free-free Euler–Bernoulli beam. The kinematics equations of the position and attitude of the airship are [3]:

$$\begin{cases} \dot{\xi} = R(\eta)v_a + v_w \\ \dot{\eta} = J(\eta)\Omega \end{cases} \quad (4)$$

where $\xi = [x, y, z]^T$ is the position vector, $\eta = [\phi \ \theta \ \psi]^T$ is the attitude vector, $v_a = [u, v, w]^T$ is the translational velocity vector in F_b , and v_w is the wind velocity in fixed frame. From Equation (4), it can be obtained that the local velocity is:

$$v = v_a + R^T(\eta) \cdot v_w \quad (5)$$

where $R(\eta)$ denotes the direction cosine matrix [3], and the transformation matrix J is:

$$J(\eta) = \begin{pmatrix} 1 & s(\phi) \tan \theta & c(\phi) \tan \theta \\ 0 & c(\phi) & -s(\phi) \\ 0 & s(\phi) \sec \theta & c(\phi) \sec \theta \end{pmatrix} \quad (6)$$

where $|\theta| < \pi/2$ is assumed to avoid the matrix singularity, and $s(\cdot)$ and $c(\cdot)$ denote sine and cosine functions, respectively.

The motions of the flexible airship are described as Lagrange equations [24], and the flexible dynamics model is obtained as follows [21]:

$$M_{sys} \begin{bmatrix} \dot{v}_a \\ \dot{\Omega} \\ \ddot{q} \end{bmatrix} = - \begin{bmatrix} 0 \\ 0 \\ S_E \end{bmatrix} + \begin{bmatrix} F_I \\ M_I \\ Q_I \end{bmatrix} + \begin{bmatrix} F_G \\ M_G \\ Q_G \end{bmatrix} + \begin{bmatrix} F_{AS} \\ M_{AS} \\ Q_{AS} \end{bmatrix} + \begin{bmatrix} F_{AD} \\ M_{AD} \\ Q_{AD} \end{bmatrix} + \begin{bmatrix} F_C \\ M_C \\ Q_C \end{bmatrix} \quad (7)$$

where $M_{sys} = \begin{bmatrix} M_{11} & M_{12} & M_{13} \\ M_{21} & M_{22} & M_{23} \\ M_{31} & M_{32} & M_{33} \end{bmatrix}$ is the airship total mass, the virtual mass terms are included, F_I denotes the inertia force vector, F_G denotes the gravity vector, F_{AS} denotes the aerostatic force vector, F_{AD} denotes the aerodynamics force vector, and F_C denotes the control force vector; M_i and Q_i denote the associated moments and general elastic forces of the flexible airship, $i = I, G, AS, AD$ and C . The local velocity is as Equation (5); $q = [q_1, q_2, \dots, q_{2N}]^T$ denotes the generalized elastic coordinate vector. S_E denotes the internal elastic force vector,

$$S_E = Kq \quad (8)$$

where the stiffness matrix K meets

$$K_{i,j} = K_{N+i,N+j} = \int_L EI \cdot \Phi_i'' \Phi_j'' dx, (i, j = 1, 2, \dots, N) \quad (9)$$

where $\Phi_i'' = \frac{d^2\Phi_i}{dx^2}$. EI denotes bending stiffness with $EI = \pi R^3 ET_0$, E is the elastic modulus of the hull envelope, T_0 is its thickness, and R is the hull radius. Equation (7) can be rewritten as

$$\dot{X}(t) = f(X) + g(X)u(t) \tag{10}$$

where $X = [\mathbf{v}_a^T \quad \Omega^T \quad \dot{q}^T]^T$ is the augmented state vector, $u = [\delta_T \quad \delta_e \quad \delta_r]^T$ denote control inputs of the thruster, elevator, and rudder, and

$$f = \frac{1}{M_{sys}} \left(- \begin{bmatrix} 0 \\ 0 \\ \mathbf{S}_E \end{bmatrix} + \begin{bmatrix} \mathbf{F}_I \\ \mathbf{M}_I \\ \mathbf{Q}_I \end{bmatrix} + \begin{bmatrix} \mathbf{F}_G \\ \mathbf{M}_G \\ \mathbf{Q}_G \end{bmatrix} + \begin{bmatrix} \mathbf{F}_{AS} \\ \mathbf{M}_{AS} \\ \mathbf{Q}_{AS} \end{bmatrix} + \begin{bmatrix} \mathbf{F}_{AD} \\ \mathbf{M}_{AD} \\ \mathbf{Q}_{AD} \end{bmatrix} \right) \tag{11}$$

$$g = [g_1 \quad g_2 \quad g_3]_{9 \times 3} \tag{12}$$

$$g_1 = \frac{1}{M_{sys}} \begin{bmatrix} \bar{F}_{kT} \\ \left(S_T + \sum_{i=1}^{2N} q_i S_{\Phi_i} \right) \bar{F}_{kT} \\ \bar{F}_{kT}^T [\Phi_{xi} \quad \Phi_{yi} \quad \Phi_{zi}]^T \end{bmatrix}_{9 \times 1}, \quad g_2 = \frac{1}{M_{sys}} \begin{bmatrix} \bar{F}_{\delta_e} \\ \left(S_f + \sum_{i=1}^{2N} q_i S_{\Phi_i} \right) \bar{F}_{\delta_e} \\ \bar{F}_{\delta_e}^T [\Phi_{xi} \quad \Phi_{yi} \quad \Phi_{zi}]^T \end{bmatrix}_{9 \times 1}, \quad g_3 = \frac{1}{M_{sys}} \begin{bmatrix} \bar{F}_{\delta_r} \\ \left(S_f + \sum_{i=1}^{2N} q_i S_{\Phi_i} \right) \bar{F}_{\delta_r} \\ \bar{F}_{\delta_r}^T [\Phi_{xi} \quad \Phi_{yi} \quad \Phi_{zi}]^T \end{bmatrix}_{9 \times 1}, \tag{13}$$

$$S_T = \begin{bmatrix} 0 & -z_T & y_T \\ z_T & 0 & -x_T \\ -y_T & x_T & 0 \end{bmatrix}, \quad S_{\Phi_i} = \begin{bmatrix} 0 & -\Phi_{zi} & \Phi_{yi} \\ \Phi_{zi} & 0 & -\Phi_{xi} \\ -\Phi_{yi} & \Phi_{xi} & 0 \end{bmatrix}, \quad S_f = \begin{bmatrix} 0 & -z_r & y_r \\ z_r & 0 & x_r - x_m \\ -y_r & -x_r + x_m & 0 \end{bmatrix}, \tag{14}$$

$$\bar{F}_{kT} = [k_T \quad 0 \quad 0]^T, \quad \bar{F}_{\delta_e} = \bar{q} S_{ref} [0 \quad 0 \quad C_{z\delta_e}]^T, \quad \bar{F}_{\delta_r} = \bar{q} S_{ref} [0 \quad C_{y\delta_r} \quad 0]^T, \tag{15}$$

where (x_T, y_T, z_T) and (x_r, y_r, z_r) denote positions of the thrust and control surface in the body frame, \mathbf{F}_b , respectively; x_m is the position of the aerostatic center along the x-axis, k_T is control gain for thruster. $C_{z\delta_e}$ and $C_{y\delta_r}$ denote the aerodynamic derivative coefficients of the elevator and rudder, respectively, $\bar{q} = \frac{1}{2}\rho V^2$ denotes the dynamic pressure, V is the airspeed, and ρ is the air density.

Next, we detailed and present each force and moment on the right-hand side of Equation (11). The inertia force and moment vector of the flexible airship in Equation (11) is [21]:

$$\begin{bmatrix} \mathbf{F}_I \\ \mathbf{M}_I \\ \mathbf{Q}_I \end{bmatrix} = - \begin{bmatrix} m\Omega^\times & -\Omega^\times \mathbf{c}_{total}^\times & 2\mathbf{P}_{\dot{q}} \\ \mathbf{c}_{total}^\times \Omega^\times & \Omega^\times \mathbf{J}_{total} & 2\mathbf{H}_{\dot{q},total} \\ -\mathbf{P}_{\dot{q}}^T & -\mathbf{H}_{\dot{q},total}^T & 2\mathbf{M}_{e\dot{q}} \end{bmatrix} \begin{bmatrix} \mathbf{v}_a \\ \Omega \\ \dot{q} \end{bmatrix} \tag{16}$$

where

$$\begin{aligned} \mathbf{c}_{total}^\times &= \mathbf{M}_{21} = \left(\int_m (\mathbf{r} + \mathbf{u}) dm \right)^\times = \left(m\mathbf{r}_G + \int_m (\sum q_i(t) \Phi_i(\mathbf{r})) dm \right)^\times, \quad \mathbf{J}_{total} = \mathbf{M}_{22} = - \int_m (\mathbf{r} + \mathbf{u})^\times (\mathbf{r} + \mathbf{u})^\times dm, \\ \mathbf{P}_{\dot{q}} &= \Omega^\times \mathbf{P} = \Omega^\times \mathbf{M}_{13}, \quad \mathbf{H}_{\dot{q}} = \left[\mathbf{J}'_{ru,1} \Omega \quad \mathbf{J}'_{ru,2} \Omega \quad \cdots \quad \mathbf{J}'_{ru,2N} \Omega \right], \quad \mathbf{J}'_{ru,i} = \int_m \mathbf{r}^\times \Phi_i^\times dm, \quad \mathbf{H}_{\dot{q},total} = \mathbf{H}_{\dot{q}} + \mathbf{H}_{\dot{q}u}, \\ \mathbf{H}_{\dot{q}u} &= \left[\sum q_j(t) \mathbf{J}''_{uu,1j} \Omega \quad \sum q_j(t) \mathbf{J}''_{uu,2j} \Omega \quad \cdots \quad \sum q_j(t) \mathbf{J}''_{uu,2Nj} \Omega \right] (i, j = 1, 2, \dots, 2N), \quad \mathbf{M}_{e\dot{q}} = \int_m \Phi^T \Omega^\times \Phi dm. \end{aligned} \tag{17}$$

The superscript denotes the skew-symmetric matrix form of a vector (corresponding to a cross-product operation). Consider the gravity, aerostatic force, and moment vector of the flexible airship in Equation (11). Gravity, the resulted moment, and its generalized one are described as follows:

$$\mathbf{F}_G = mg\hat{\mathbf{g}} \tag{18}$$

$$\mathbf{M}_G = (\mathbf{r}_G + \mathbf{u}_G) \times \mathbf{F}_G = \mathbf{r}_G \times \mathbf{F}_G + \frac{1}{m} \sum_{i=1}^{2N} q_i(t) \mathbf{p}_i \times \mathbf{F}_G \tag{19}$$

$$Q_{Gi} = \int_m \mathbf{g} \hat{\mathbf{g}}^T \Phi_i dm = \mathbf{g} \hat{\mathbf{g}}^T \mathbf{p}_i, i = 1, 2, \dots, 2N \tag{20}$$

where g denotes that the acceleration of gravity and unit direction vector of gravity is:

$$\hat{\mathbf{g}} = [-\sin \theta \quad \cos \theta \sin \phi \quad \cos \theta \cos \phi]^T \tag{21}$$

$$\mathbf{u}_G = \int_m \mathbf{u} dm / m = \frac{1}{m} \sum_{i=1}^{2N} q_i(t) \mathbf{p}_i, \mathbf{p}_i = \int_m \Phi_i dm \tag{22}$$

The aerostatic force in the body frame in Equation (11) is:

$$\mathbf{F}_{AS} = -\rho g V_B \hat{\mathbf{g}} \tag{23}$$

The resulted moment and its generalized moment are presented as follows:

$$\mathbf{M}_{AS} = \mathbf{u}_V \times \mathbf{F}_{AS} = \left(\int_{V_B} \mathbf{u} dV / V_B \right) \times \mathbf{F}_{AS} = \sum q_i(t) \mathbf{I}_{AS,i}^\times \mathbf{F}_{AS} \tag{24}$$

$$Q_{AS,i} = - \int_L \rho \mathbf{g} \hat{\mathbf{g}}^T \Phi_i S dx = \mathbf{F}_{AS}^T \mathbf{I}_{AS,i}, i = 1, 2, \dots, 2N \tag{25}$$

where V_B denotes the volume of the airship hull and S is the hull cross-sectional area:

$$\mathbf{u}_V = \frac{1}{V_B} \int_{V_B} \mathbf{u} dV, \mathbf{I}_{AS,i}^\times = \frac{1}{V_B} \int_{V_B} \Phi_i dV = \frac{1}{V_B} \int_L \Phi_i S(x) dx \tag{26}$$

The aerodynamics force and moment vector of the flexible airship in Equation (11) is:

$$\begin{bmatrix} \mathbf{F}_{AD} \\ \mathbf{M}_{AD} \\ \mathbf{Q}_{AD} \end{bmatrix} = \begin{bmatrix} \mathbf{F}_p \\ \mathbf{M}_p \\ \mathbf{Q}_p \end{bmatrix} + \begin{bmatrix} \mathbf{F}_v \\ \mathbf{M}_v \\ \mathbf{Q}_v \end{bmatrix} + \begin{bmatrix} \mathbf{F}_F \\ \mathbf{M}_F \\ \mathbf{Q}_F \end{bmatrix} + \begin{bmatrix} \mathbf{F}_{H(F)} \\ \mathbf{M}_{H(F)} \\ \mathbf{Q}_{H(F)} \end{bmatrix} + \begin{bmatrix} \mathbf{F}_{axial} \\ \mathbf{M}_{axial} \\ \mathbf{Q}_{axial} \end{bmatrix} \tag{27}$$

where subscripts $p, v, F, H(F)$, and the axial on the right-hand side of Equation (27) denote the forces and moments due to the potential-flow (related to the added mass), viscous effect on the hull, aerodynamic force acting on fins and acting on the hull due to the fins, and axial drag, respectively. The calculation of the aerodynamics forces is the same as in [21].

The control force and moment vector $\mathbf{F}_C, \mathbf{M}_C, \mathbf{Q}_C$ of the flexible airship includes those of propellers and control surface deflections. The thrust in the body frame is $\mathbf{F}_T = [F_{Tx} \quad F_{Ty} \quad F_{Tz}]^T$; the corresponding moment and generalized moment are as follows:

$$\mathbf{M}_T = \mathbf{r}_T \times \mathbf{F}_T + \sum q_i(t) \Phi_i(\mathbf{r}_T) \times \mathbf{F}_T \tag{28}$$

$$Q_{Ti} = \mathbf{F}_T \Phi_i(\mathbf{r}_T) \tag{29}$$

where $\Phi_i(\mathbf{r}_T)$ is the mode shape function at the propeller-mounted position \mathbf{r}_T . Forces due to the control surface deflection are presented in the body frame, as

$$\mathbf{F}_\delta^T = \begin{bmatrix} \Delta C_D \\ \Delta C_L(\delta_r) \\ \Delta C_L(\delta_e) \end{bmatrix} \cdot \bar{q} \cdot S_f \tag{30}$$

where S_f denotes the area of control surface, and ΔC_L and ΔC_D are the lift and drag resulted from the control surface deflection. The corresponding moment and generalized moment are:

$$\mathbf{M}_\delta = \mathbf{r}_\delta \times \mathbf{F}_\delta + \sum q_i(t) \Phi_i(\mathbf{r}_\delta) \times \mathbf{F}_\delta \tag{31}$$

$$Q_{\delta,i} = \mathbf{F}_\delta^T \Phi_i(\mathbf{r}_\delta) \tag{32}$$

where $\Phi_i(\mathbf{r}_\delta)$ is the shape function at the control surface-mounted position of \mathbf{r}_δ .

Considering the model uncertainties or disturbances often occurring in the dynamics system of Equation (10), assume the atmospheric parameters are stable and disturbances are bounded; thus, a model uncertainty, \mathbf{d} , and the actuator saturation are introduced, thus the system (10) can be modified, as

$$\dot{\mathbf{X}}(t) = \mathbf{f}(\mathbf{X}) + \mathbf{g}(\mathbf{X})\text{sat}(\mathbf{u}_a(t)) + \mathbf{\Gamma}\mathbf{d}(t) \tag{33}$$

where \mathbf{d} denotes disturbances except for winds and model uncertainties, such as aerodynamic coefficients and structural stiffness; $\text{sat}(\cdot)$ denotes saturation function. As the airship has a large inertia and its motion is slow and sedate, \mathbf{d} can be assumed to be a slow-varying disturbance, which can be estimated on-line by using an adaptive law. Let $\hat{\mathbf{d}}$ be the estimated value of the uncertain parameter \mathbf{d} ; $\tilde{\mathbf{d}} = \hat{\mathbf{d}} - \mathbf{d}$ is the associated estimated error. Finally, $\mathbf{\Gamma}$ denotes the disturbance coefficient matrix. The faults can be modeled as abrupt changes of the nominal control action from \mathbf{u}_a [26,27],

$$\mathbf{u}_a^f(t) = \mathbf{u}_a(t) + (\mathbf{I} - \bar{\rho}_a(t))(\mathbf{f}_a(t) - \mathbf{u}_a(t)) \tag{34}$$

that is,

$$\mathbf{u}_a^f(t) = \mathbf{u}_h + \mathbf{u}_f = \underbrace{\bar{\rho}_a \mathbf{u}_a(t)}_{\mathbf{u}_h} + \underbrace{(\mathbf{I} - \bar{\rho}_a(t))\mathbf{f}_a(t)}_{\mathbf{u}_f} \tag{35}$$

where $\mathbf{u}_a = [u_{a,1}, u_{a,2}, \dots, u_{a,m}] \in R^m$ is the actual control output; the diagonal matrix $\bar{\rho}_a = \text{diag}\{\rho_{a,1}, \rho_{a,2}, \dots, \rho_{a,m}\}$ denotes the operational effectiveness of the actuators; \mathbf{I} is the $m \times m$ identity matrix; the fault vector $\mathbf{f}_a = [f_{a,1}, f_{a,2}, \dots, f_{a,m}] \in R^m$ denotes the control action from the failed or un-manipulated actuators; $\mathbf{u}_h = \bar{\rho}_a \mathbf{u}_a(t)$ denotes the remaining control of the health actuators; $\mathbf{u}_f = (\mathbf{I} - \bar{\rho}_a(t))\mathbf{f}_a(t)$ denotes the fault of the inputs.

Assumption 1. In Equation (34), for the multiplicative and additive actuator faults, $\rho_{a,i}$ and $f_{a,i}$ are all bounded. In addition, $\dot{\rho}_{a,i}$ and $\dot{f}_{a,i}$ exist and are bounded, $i = 1, 2, \dots, m$.

Substituting Equation (35) into Equation (33) yields:

$$\dot{\mathbf{X}}(t) = \mathbf{f}(\mathbf{X}) + \mathbf{g}(\mathbf{X})\bar{\rho}_a \text{sat}(\mathbf{u}_a(t)) + \mathbf{g}(\mathbf{X})(\mathbf{I} - \bar{\rho}_a(t))\mathbf{f}_a(t) + \mathbf{\Gamma}\mathbf{d} \tag{36}$$

Remark 1. There are two underactuated cases for the flexible airship. Case 1. The airship without a lateral tilt angle of the propellers (i.e., the thrust direction is fixed) is underactuated in the y -direction (that is, the lateral control force, $T_{sy} = 0$); thus, the sway velocity, v , cannot be directly controlled. If the wind is in the presence in this case, then the airship can align against the wind through the yaw motion, reducing the lateral forces requirement to a low and acceptable value; thus, the lateral force input can vanish in stationary conditions. Case 2. The airship works in Case 1 without ailerons or differential actuators (i.e., $\delta_{eL} = \delta_{eR}$, $\delta r_U = \delta r_B$, and the roll control moment, $M_{Tx} \approx 0$). Sway velocity, v , and bank angle, φ , cannot be directly controlled. In this case, the disturbance of the roll moment resulting from the wind can be attenuated by the airship roll damp; thus, the roll moment input can vanish in stationary conditions.

2.2. Fault Tolerant Trajectory Tracking Problem

The fault-tolerant trajectory tracking problem is a challenge for the flexible stratospheric airship because it is a hard task to achieve precise trajectory tracking under the actuator faults; the main reason is that the interaction between fluid and structure should be considered. Presently, consider the system of Equations (10) and (36)—the control task is to design a fault-tolerant trajectory-tracking controller, such that the closed-loop system is globally asymptotically stable and the output trajectory, η , is steered towards a given reference trajectory, η_r , with $\lim_{t \rightarrow \infty} \|e(t)\|_2 < \varepsilon_0$, even in a specified model parameter uncertainty, unknown wind disturbances, and control surface faults; where the tracking error is $e(t) = \eta(t) - \eta_r(t)$, ε_0 is a prescribed constant, and 2-norm is $\|e(t)\|_2 = \sqrt{e^T e}$.

3. BNTSM-Based Trajectory Tracking Design

In this section, the robust BNTSM controller is designed to solve the problem in Section 2.2. Firstly, a command filter is used to meet the magnitude and rate constraints of the input signal. The command filter can be obtained by using a second-order lower pass filter, as follows:

$$G_r(s) = \frac{X_r(s)}{X_r^0(s)} = \frac{\omega_n^2}{s^2 + 2\zeta_n \omega_n s + \omega_n^2} \tag{37}$$

where ζ_n denotes the filter-damping ratio and ω_n denotes the undamped nature frequency of the filter. To reduce the filter error $e = x_r^0 - x_r$, the filter frequency, ω_n , is the bandwidth of $X_r^0(s)$, which is generally less than that of $G_r(s)$, and then ω_n can be selected.

Secondly, for the system (4), the wind field is assumed as a constant, due to the stable meteorological condition in the stratosphere [28]. Some people regarded wind speed as one kind of external disturbance, but it is hard to separate wind and model uncertainty and they are not easily handled. Here, a wind observer is introduced to improve tracking performances. A wind observer state is defined, $[\hat{\xi}^T \ \hat{v}_w^T]^T$, where $\hat{\xi}$ and \hat{v}_w denote estimates of ξ and v_w . The wind can be sensed by the wind speed sensors in the fixed frame, and the observer dynamics are designed, as follows [4]:

$$\begin{bmatrix} \dot{\hat{\xi}} \\ \dot{\hat{v}}_w \end{bmatrix} = \begin{bmatrix} \mathbf{R}(\eta)v_a \\ 0 \end{bmatrix} + \begin{bmatrix} L_{\xi} & I_3 \\ L_w & 0 \end{bmatrix} \begin{bmatrix} \xi - \hat{\xi} \\ \hat{v}_w \end{bmatrix} \tag{38}$$

The estimation error of the position and wind speed are defined as $e_4 = \begin{bmatrix} \xi - \hat{\xi} \\ v_w - \hat{v}_w \end{bmatrix}$, and the estimation error e_4 can be obtained as

$$\dot{e}_4 = \begin{bmatrix} \xi - \hat{\xi} \\ v_w - \hat{v}_w \end{bmatrix} = \begin{bmatrix} -L_{\xi} & I_3 \\ -L_w & 0 \end{bmatrix} e_4 = \tilde{A}_e e_4 \tag{39}$$

where L_{ξ} , L_w are gain matrices such that $\tilde{A}_e = \begin{bmatrix} -L_{\xi} & I_3 \\ -L_w & 0 \end{bmatrix}$ be Hurwitz; I_3 is the unit matrix with a dimension of 3×3 . Thus, there exists a positive definite symmetrical matrix, P_e , such that

$$\frac{d}{dt} (e_4^T P_e e_4) = -e_4^T Q_e e_4 \tag{40}$$

where $Q_e = \text{diag}(Q_{\xi}, Q_{v_w})$, Q_{ξ} , and Q_{v_w} are symmetric positive definite matrices and the weight matrix, P_e , meets the following Lyapunov equation,

$$\tilde{A}_e^T P_e + P_e \tilde{A}_e = -Q_e \tag{41}$$

Thirdly, consider the kinematics in Equation (4) and dynamics in Equation (36). The control objective is to track a reference signal, $x_{1r} = \eta_r$, with the derivative \dot{x}_{1r} under unknown disturbances and faults. The tracking error vectors of the attitudes are defined as

$$z_1 = x_1 - x_{1r} \tag{42}$$

$$z_2 = x_2 - x_{2r} \tag{43}$$

where $x_1 = \eta$, $x_2 = \dot{x}_1 = \dot{\eta}$, x_{1r} is the reference or desired attitude angle, and x_{2r} is the output of a command filter.

Presently, the BNTSM controller is designed, and the kinematics Equation (4) and dynamics Equation (33) are considered. To obtain a fast and transient response and finite time convergence without a singular problem, a non-singular terminal sliding-mode (NTSM) surface or manifold is designed by using the fractional order derivative, as follows [29],[30]:

$$s = \tilde{z}_1 + \alpha_\gamma \tilde{z}_1^\lambda + \frac{1}{\beta} \tilde{z}_2^{p/q} = \tilde{z}_1 + \alpha_\gamma \left| \tilde{z}_1 \right|^\lambda \text{sgn}(\tilde{z}_1) + \frac{1}{\beta} \left| \tilde{z}_2 \right|^{p/q} \text{sgn}(\tilde{z}_2) \tag{44}$$

where \tilde{z}_1 and \tilde{z}_2 are defined in (A6), the SMC parameter $\lambda > p/q$, $\alpha_\gamma > 0$, $s = [s_1 \ s_2 \ s_3]^T \in R^3$ denotes the sliding-mode surface, i.e., $s_1 = s(\varphi)$, $s_2 = s(\theta)$, $s_3 = s(\psi)$ and $1 < p/q < 2$, $\beta > 0$; $\text{sgn}(\cdot)$ is the sign function. In addition, the derivative of the sliding-mode surface, s , is

$$\dot{s} = \dot{\tilde{z}}_1 + \alpha_\gamma \lambda \left| \tilde{z}_1 \right|^{\lambda-1} \cdot \dot{\tilde{z}}_1 + \frac{1}{\beta} \cdot \frac{p}{q} \left| \tilde{z}_2 \right|^{(p/q)-1} \cdot \dot{\tilde{z}}_2 \tag{45}$$

Using an extended CLF, a control law will be designed to drive the virtual angular rate error, \tilde{z}_2 , to zero, while ensuring that the current attitude vector, η , will converge to the desired value of η_r . The attitude controller is derived in two steps, and the detailed design is presented in Appendix A.

Presently, we consider the input saturation problem, in order to analyze the effect of the actuator saturation on the closed-loop dynamics; the actuator output is

$$\text{sat}(u_a) = \begin{cases} u_a^{f0} + \hat{u}_f & \text{for } \left| u_a^{f0} + \hat{u}_f \right| < U_{\text{lim}} \\ U_{\text{lim}} & \text{for } u_a^{f0} + \hat{u}_f > U_{\text{lim}} \\ -U_{\text{lim}} & \text{for } u_a^{f0} + \hat{u}_f < -U_{\text{lim}} \end{cases} \tag{46}$$

where u_a^{f0} is the input of the BNTSM controller as Equation (A13), and \hat{u}_f is the fault estimator as Equation (A19).

Furthermore, defining Δu as the difference between the desired control input u and the actuator output, i.e., $\Delta u = u_a - \text{sat}(u_a)$, an anti-windup compensator is designed to compensate for the actuator saturation, as follows:

$$v = K_s(u_a - \text{sat}(u_a)) \tag{47}$$

where K_s is the control gain of the saturation compensator, and then the total control is

$$u_a = u_a^{f0} + \hat{u}_f + v \tag{48}$$

Remark 2. For the fault estimator (A19) (in Appendix A), if \tilde{z}_2 converges to zero, then \hat{u}_f will converge to zero, and the fault becomes constant; a disturbance observer method [31] can be used to estimate $\hat{u}_f = \text{const}$.

This scenario will demonstrate the attitude-tracking performance by using the proposed BNTSM controller and the wind observer. The wind vector is initially set as

$$v_w = \begin{cases} [7, 0, 0]^T \text{ (m/s)}, t \leq 20\text{s} \\ [0, 5, 0]^T \text{ (m/s)}, 20\text{s} < t \leq 50\text{s} \\ [0, 0, 3]^T \text{ (m/s)}, 50\text{s} < t \leq 80\text{s} \\ [3, 1, 2]^T \text{ (m/s)}, t > 80\text{s} \end{cases} \quad (49)$$

Wind parameters in (38) and (39) are chosen as $L_{\zeta} = \text{diag}(1, 1, 1)$, $L_w = \text{diag}(2.5, 2.5, 2.5)$, and $Q_{\zeta} = I_3$, $Q_{v_w} = I_3$. To illustrate the proposed performances, a backstepping integral sliding-mode control (BISMIC) [3,4] and a PID controller are employed for comparison. The sliding surface s of the BISMIC is defined as follows: $s = \lambda_1 z_1 + \lambda_2 \int_0^t z_1 d(t) + z_2$. In addition, the PID controller structure is as in Figure 3.

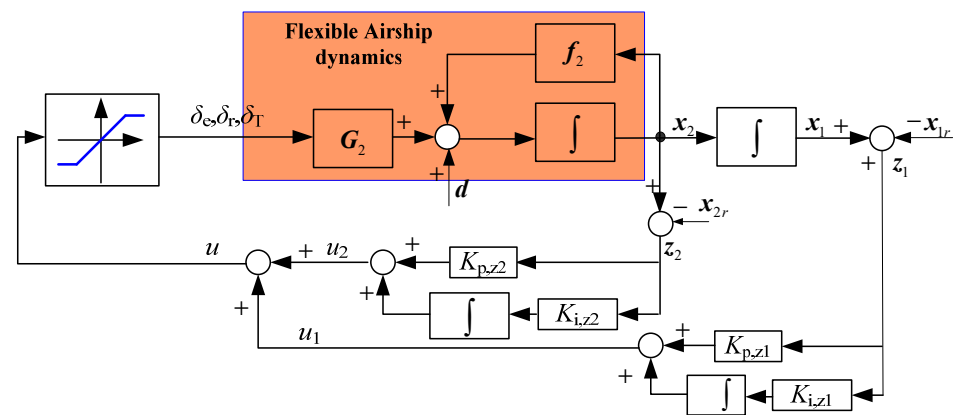


Figure 3. The PID controller configuration.

The controller parameters are designed as shown in Table 2.

Table 2. Selected parameters of the controller.

Controller	Parameters	Value
PID	$k_{p,zj}, k_{i,zj} (j = 1, 2)$	2, 0.04
BNTSM	c_1, c_2	$\text{diag}(2, 2, 2), \text{diag}(0.2, 0.2, 0.2)$
	h, ζ, φ_s	$0.01 * \text{diag}(1,1,1), 0.01 * \text{diag}(1, 1.2, 1), 0.4$
	p, q, β	$5, 3, 0.1 * \text{diag}(1, 1, 1)$
	$\alpha_r, \gamma_d, \lambda$	$5, 1, 1.8 * \text{diag}(1, 1, 1)$
BISMIC	c_1, c_2	$0.1 * \text{diag}(1, 1, 1), 0.01 * \text{diag}(1, 1, 1)$
	h, ζ	$0.1 * \text{diag}(1, 1, 1), \text{diag}(1, 1.2, 1)$
	λ_1, λ_2	$0.5 * \text{diag}(1, 1, 1), 0.05 * \text{diag}(1, 1, 1)$
	$\varphi_s, k_{i,smc}$	0.4, 0.1

The parameters are selected to satisfy the requirements in Section 3 after several design iterations. The damping ratio and undamped nature frequency of the command filter are selected as $\zeta_n = 0.9$, $\omega_n = 20$ rad/s. The mode number, N, selects $N = 2$, $P_e = 0.1$, $\Gamma = 1$. The gain of the actuator saturation compensator is $K_s = 1$, and control gain for thruster $k_T = 90,000$. A doublet command is predefined as the desired attitude.

For an easier comparison, the averaged tracking error is defined as

$$E = \sqrt{\frac{1}{N} \sum_{k=1}^N (\|e(k)\|^2)} \quad (50)$$

where N is the number of simulation steps, and the elapsed time (ET) is the time that MATLAB has used to complete the 10-s simulation time. This may not reflect the true computational burden of the controllers, but it can be used to provide a general idea about the comparison in computational time among the controllers. The simulation results are shown, as follows.

It can be observed from Figure 4 and Table 3 that the reference signals of pitch and yaw angles are precisely tracked, but the averaged tracking errors of the BNTSM controller are smallest, and then those by the BISMIC design are smaller, and the PID controller provides worse tracking performances comparing with the BNTSM control and the BISMIC. In view of the computational burden, the BNTSM controller is time consuming, while the cost of the PID controller is the cheapest. The roll motion response is free oscillating and has not been controlled due to the absence of the direct roll moment under the underactuated Case 2.

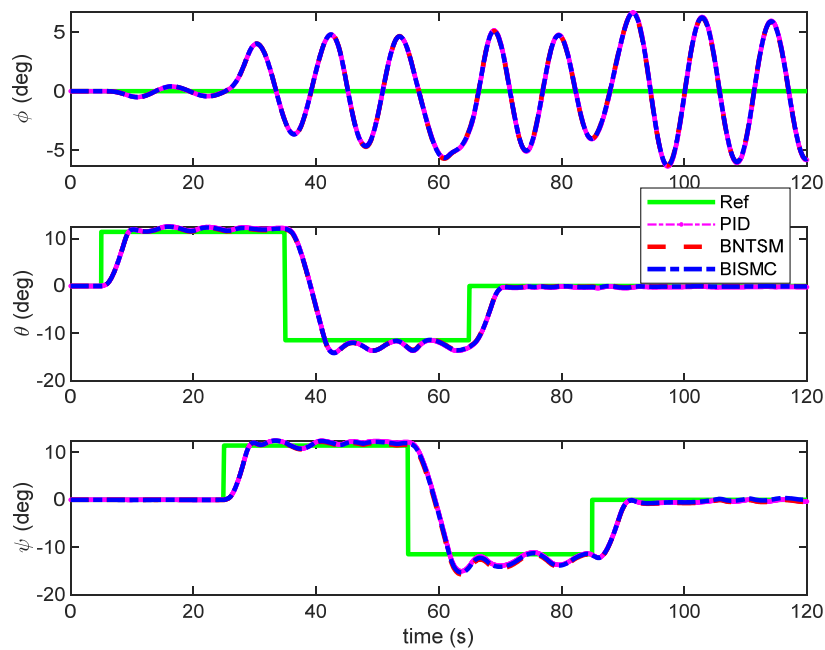


Figure 4. Euler angles in Scenario 1 without wind compensation.

Table 3. Tracking errors and ET of the airship under the input of the controller without wind compensation.

Controller Error	E_φ (rad)	E_θ (rad)	E_ψ (rad)	ET (s)
PID	0.0532	0.0843	0.0893×10^{-3}	2153.6
BNTSM	0.0525	0.0834	0.0887×10^{-3}	2367.2
BISMIC	0.0528	0.0839	0.0890×10^{-3}	2226.2

It also can be observed from Figure 5 and Tables 3 and 4 that the responses have smaller overshoots and shorter transient times by using the BNTSM controller with wind observer compensation versus those without wind compensation. The wind speeds are precisely estimated by the proposed wind observer, as shown in Figure 6. Figure 7 demonstrates the structure mode shapes in the Oxy and Oxz planes; that is, according to (3), the 1st and 2nd bending mode in the Oxy plane are $\Phi_1 = [0 \ \phi_1 \ 0]^T$ and $\Phi_2 = [0 \ \phi_2 \ 0]^T$; the 1st and 2nd bending mode in the Oxz plane are $\Phi_3 = [0 \ 0 \ \phi_1]^T$ and $\Phi_4 = [0 \ 0 \ \phi_2]^T$; the associated nature frequency of the 1st and 2nd bending modes can be obtained by the modal rigidity and mass, i.e., $\omega_{n1} = 22.8\text{rad/s}$ and $\omega_{n2} = 64.2\text{rad/s}$, respectively, and it can be observed from Figure 7 that the rigidity is bigger and the elastic displacement is smaller in the middle airship than those on the two sides of the airship.

Scenario 2. *Trajectory-tracking control under actuator faults with unknown winds.*

This scenario will demonstrate fault-tolerant tracking performance by using the proposed BNTSM controller and the fault observer. The faults of actuator bias forces with wind are studied here. The faults are set as follows: *Fault 1*, the bias from the nominal value is 5 deg and the loss of effectiveness is 25% for the elevator in $t > 30$ s; *Fault 2*, the bias from the nominal value is 5 deg and the loss of effectiveness is 50% for the rudder in $t > 60$ s. The faults are simulated by setting bias values of each actuator at the triggering time. The wind disturbances are set as Equation (49) in Scenario 1. A doublet attitude is predefined as the desired attitudes to verify the tracking performance of the BNTSM control. The controller parameters are the same as Table 2, except for

$$\begin{cases} c_2 = \text{diag}(0.2, 20, 0.2), \beta = \text{diag}(0.1, 0.002, 0.2), & \text{for BNTSM} \\ c_1 = c_2 = \text{diag}(2, 2, 2), & \text{for BISMIC} \end{cases}, \quad (51)$$

In addition, the fault observer parameters are designed as

$$\gamma_f = 3, \mathbf{P}_f = 3,000,000 \times \text{diag}(0, 1, -1). \quad (52)$$

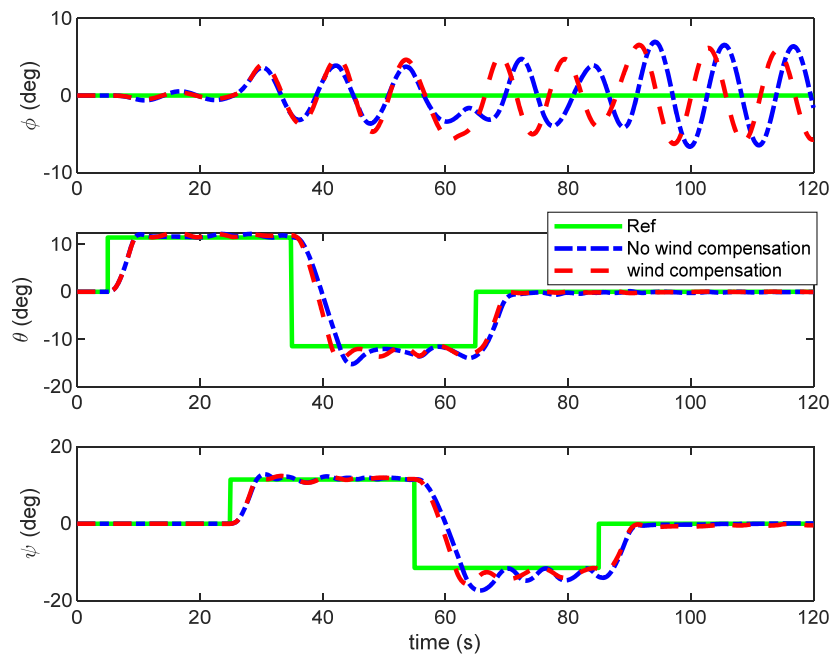


Figure 5. Tracking responses of Euler angles with and without wind compensation.

Table 4. Tracking errors and ET of the airship under the input of the controller with wind compensation.

Controller Error	E_ϕ (rad)	E_θ (rad)	E_ψ (rad)	ET (s)
PID	0.0577	0.0786	0.0817×10^{-3}	1993.2
BNTSM	0.0574	0.0774	0.0805×10^{-3}	2050.4
BISMIC	0.0575	0.0780	0.0811×10^{-3}	2048.9

By using the above design, the simulation results are demonstrated as follows.

Figures 8 and 9 shows the pitch step input of 0.2, the rad shows at 5 s, and the tracking response converges the desired value at 10 s (within 10 s). Because the doublet command is a changing signal, the steady value of the tracking response also changes; thus, the overall tracking process is dynamically varying, but the response will quickly converge when the command is fixed. It can be observed from Figure 8 and Table 5 that the reference inputs

of pitch and yaw angles are well tracked, even with control surface faults and unknown winds. Comparing with the PID controller and the BISMIC, the BNTSM controller has smaller averaged tracking errors. In the view of elapsed time, the PID controller is the least, with the BISMIC next, while the BNTSM control will cost more time. The roll motion is not controlled due to the underactuated character of the flexible airship. It also can be observed from Figure 9 and Tables 5 and 6 that the responses have shorter transient times by using the fault observer compensation and the BNTSM controller than those without fault compensation. This demonstrates the fault tolerant control capability of the BNTSM controller. The control inputs are shown in Figures 10 and 11. Figure 11 shows that the control surface faults are estimated by using the proposed estimator of (A19) (in Appendix A). There are some differences initially because the corresponding tracking errors \tilde{z}_2 are affected by the variable reference signals. The fault estimations are gradually close to the true values. Figure 12 shows the response of the sliding-mode variable, s , which asymptotically approach zero except for $s(\varphi)$, due to the underactuated roll motion.

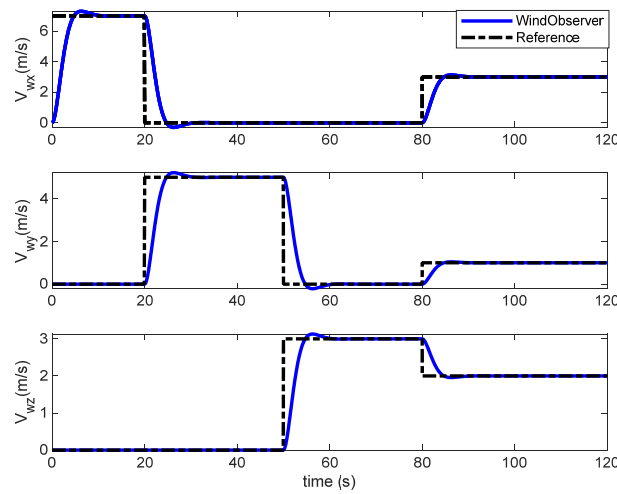


Figure 6. Wind speed estimation, in Scenario 1 with wind.

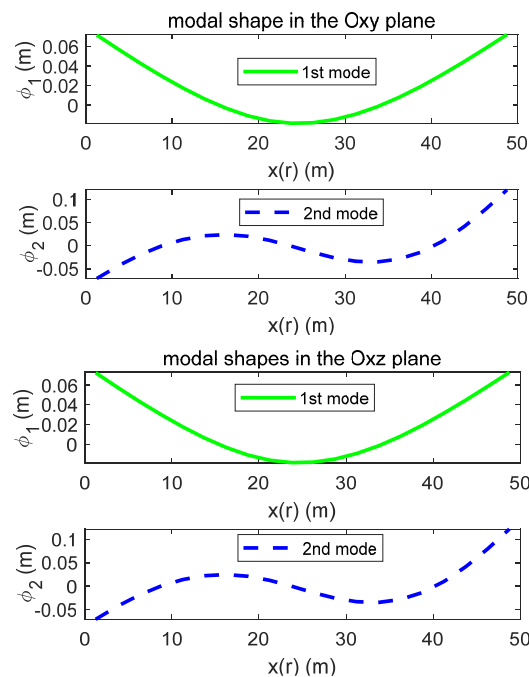


Figure 7. Structure mode shapes in the Oxy and Oxz planes.

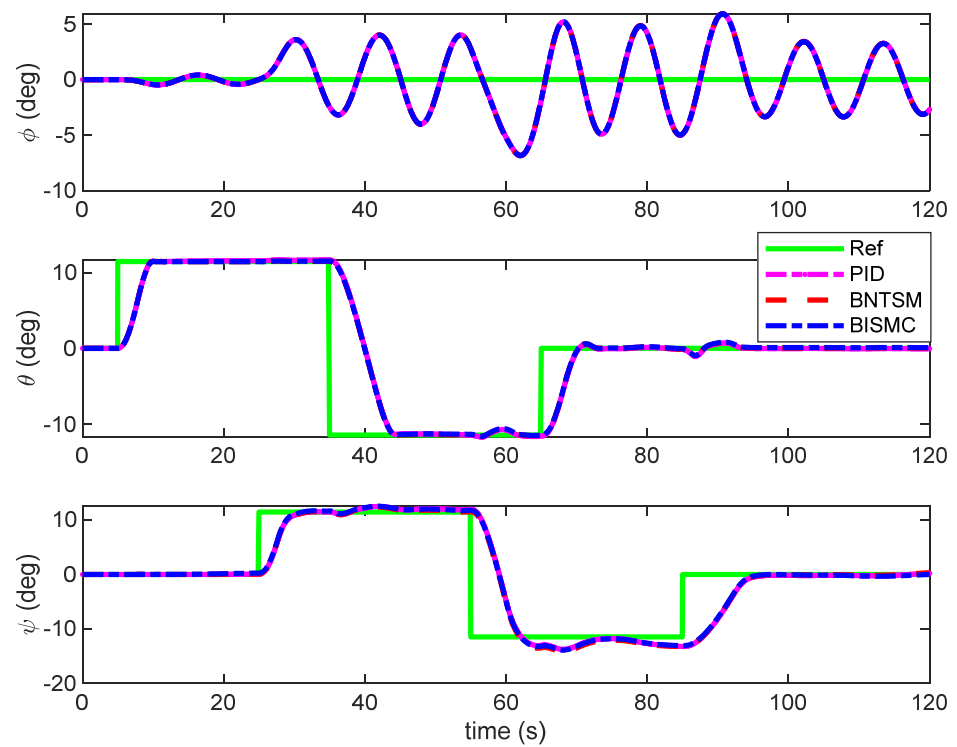


Figure 8. Attitude responses with fault compensation.

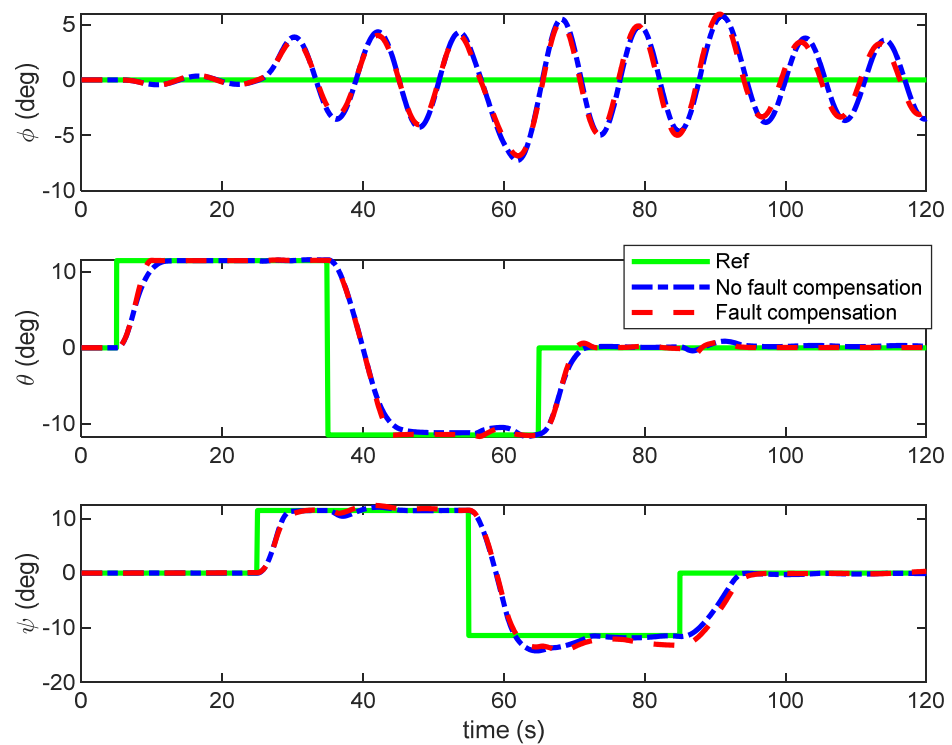


Figure 9. Tracking responses of Euler angles with and without fault compensation.

Table 5. Tracking errors and ET of the airship under the input of the controller without fault compensation.

Controller Error	E_φ (rad)	E_θ (rad)	E_ψ (rad)	ET (s)
PID	0.0510	0.0810	0.0788×10^{-3}	2171.4
BNTSM	0.0511	0.0803	0.0775×10^{-3}	2354.3
BISMIC	0.0510	0.0805	0.0780×10^{-3}	2193.0

Table 6. Tracking errors and ET of the airship under the input of the controller with fault compensation.

Controller Error	E_φ (rad)	E_θ (rad)	E_ψ (rad)	ET (s)
PID	0.0488	0.0804	0.0829×10^{-3}	1821.0
BNTSM	0.0490	0.0797	0.0817×10^{-3}	2114.1
BISMIC	0.0489	0.0798	0.0819×10^{-3}	2016.2

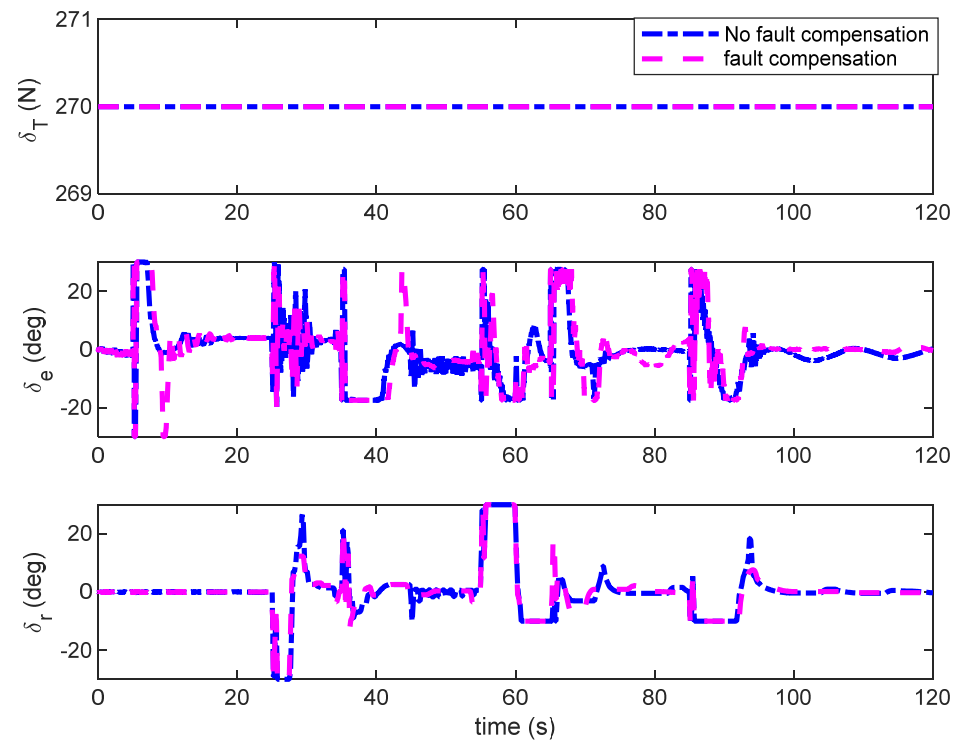


Figure 10. Control inputs with faults.

Scenario 3. Trajectory-tracking control under variable stiffness and unknown faults and winds.

In this scenario, we investigate the significance envelope flexibility has on the effect of rigid-body dynamics of the airship. What effect does the hull stiffness of the airship have on the structure modes? Four hull stiffness variants, plus the baseline stiffness case, are compared. The bending stiffness of the envelope is scaled for the model variants by $\pm 30\%$ and $\pm 50\%$, respectively. The model was trimmed in steady level flight at 9 m/s and sea level. Winds and faults are also considered as Scenario 2. The controller parameters are the same as Scenario 2 except for

$$\begin{cases} c_2 = \text{diag}(0.2, 0.2, 0.4), \beta = \text{diag}(0.1, 0.1, 0.2), \text{ for BNTSM} \\ c_1 = c_2 = \text{diag}(2, 2, 2), \text{ for BISMIC} \end{cases} \quad (53)$$

By using the BNTSM control design, the simulation results are shown in Figures 13–16.

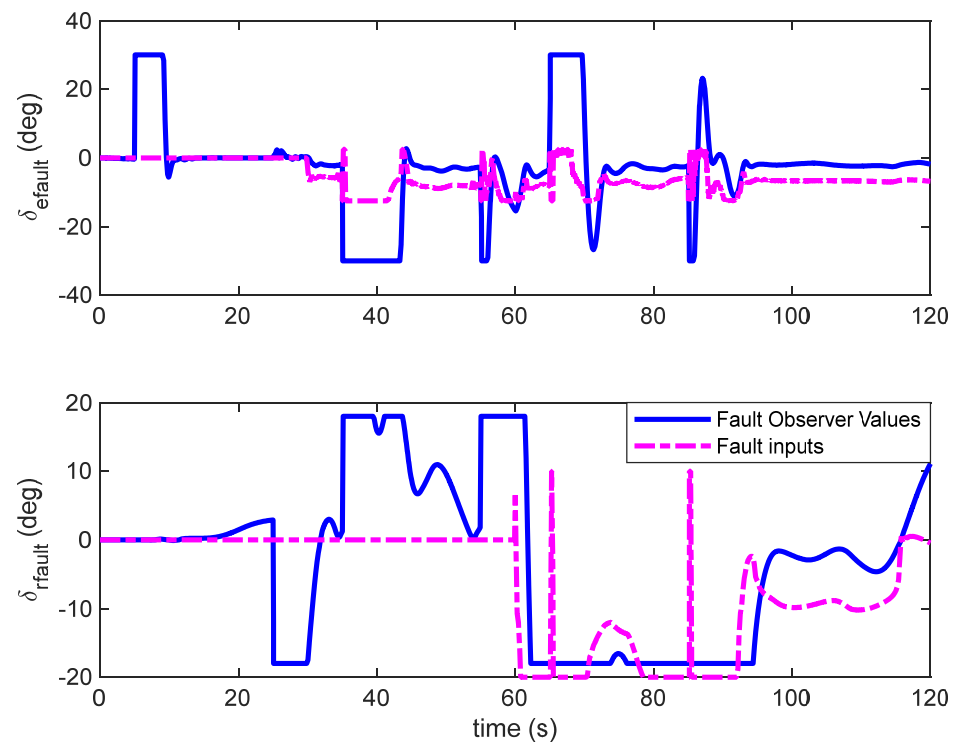


Figure 11. Control surface faults estimation.

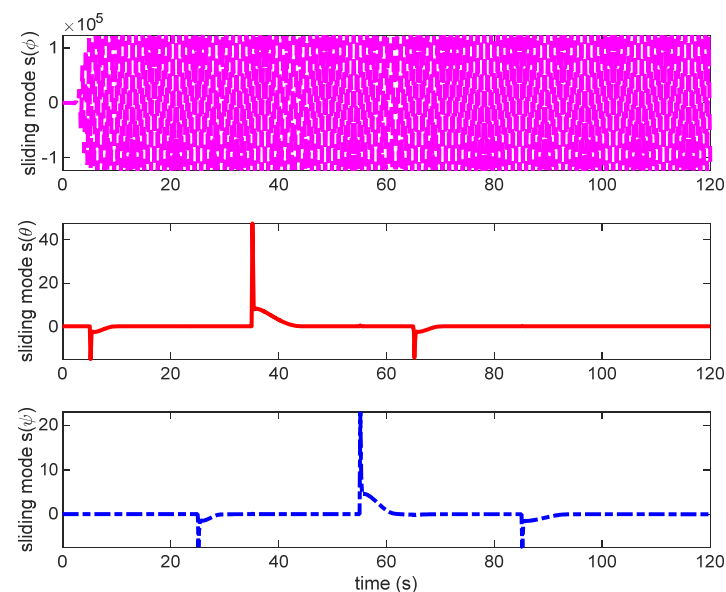


Figure 12. Response of sliding-mode variable, s .

From Figure 13, it can be observed that the variable stiffness of the airship envelope has a small effect on the rigid-body attitude and the position motions. However, the stiffness variation has a great effect on the structure modes, as shown in Figures 14 and 15, where it can be found that the bending mode responses of q_i will become a smaller and smaller amplitude of oscillation with the increasing stiffness. The general coordinate, q_1 , for the first bending mode, is increased in amplitude by 30% for the -50% stiffness variant, and the general coordinate, q_1 , reduced in amplitude by 8.3% for the $+30\%$ stiffness case. The same case happens for the generalized coordinate velocity responses. This demonstrates that stiffness can suppress structural mode oscillation. Figure 16 shows that the

control inputs change little when the stiffness of the flexible airship is variable, where * denotes multiplication sign.

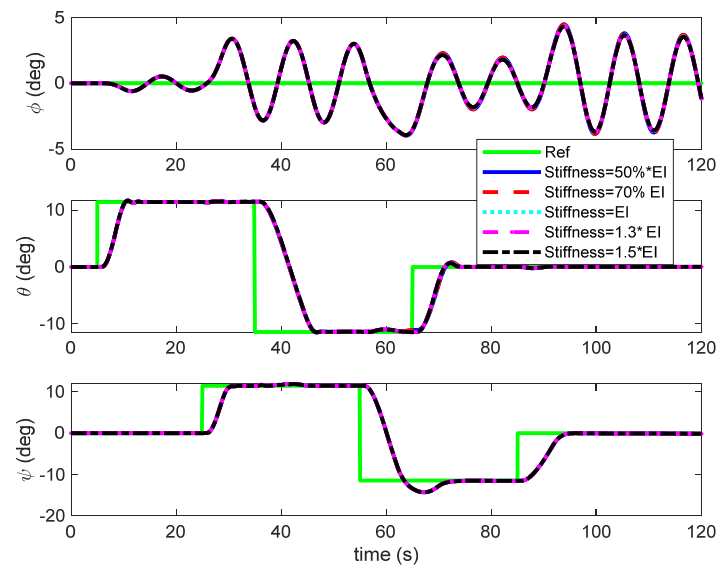


Figure 13. Attitude responses with five stiffness variants, winds and control faults.

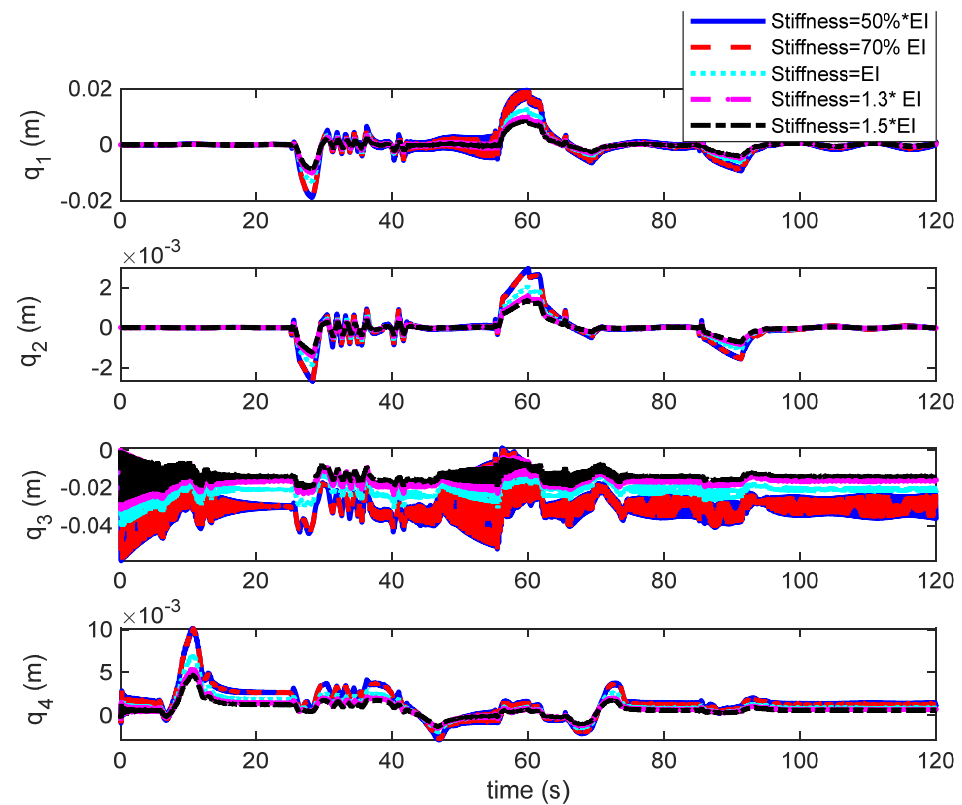


Figure 14. The generalized coordinate responses of structure modes.

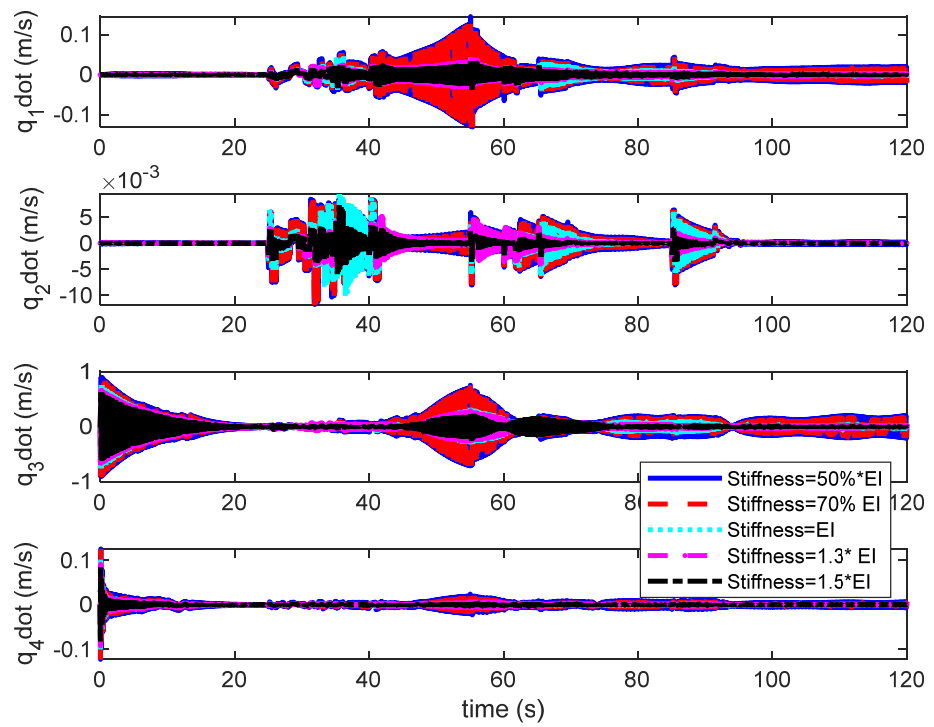


Figure 15. The generalized coordinate velocity responses of structure modes.

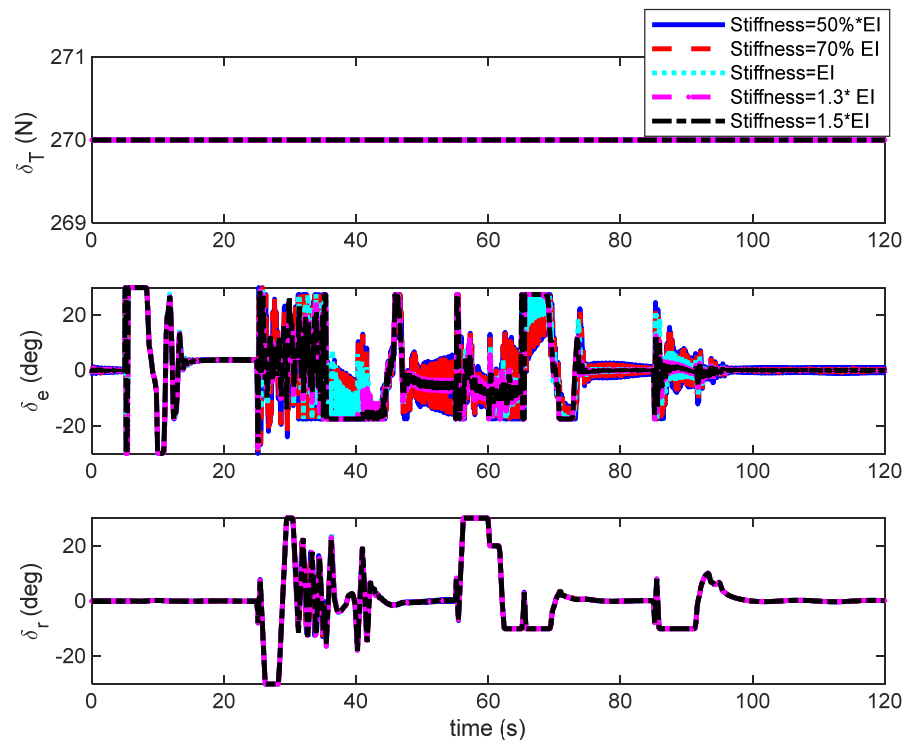


Figure 16. Control inputs with five stiffness variants.

5. Conclusions

This paper proposes a nonlinear attitude tracking control approach for the flexible airship. A nonlinear backstepping nonsingular terminal sliding-mode control method is used to design the controller to track desired attitudes and stabilize structural modes of the flexible airship. Meanwhile, a wind observer is designed to estimate variable wind speeds. An adaptive fault estimator is designed to deal with nominal offset and loss of

effectiveness faults of the control surfaces. Saturation compensator is designed to reduce effect of the actuator saturation. The stability analysis demonstrates that the closed-loop attitude tracking error dynamics are globally exponentially stable. Simulation results demonstrate that the BNTSM control designed for three scenarios of the flexible airship can achieve better attitude tracking performances by using the corresponding compensation controller, even though the airship is affected by unknown winds, control surface faults, and variable stiffness of the airship envelope. Therefore, the effectiveness and availability of the BNTSM control design are verified.

6. Future Recommendation

The future work is to expand the control strategy into a position control loop and velocity control loop for the flexible airship.

Author Contributions: Conceptualization, S.L. and J.F.W.; methodology, S.L., J.F.W., S.S. and W.L.; software, S.L. and S.S.; validation, S.L., J.F.W. and S.S.; formal analysis, J.F.W.; investigation, S.L. and W.L.; writing—original draft preparation, S.L.; writing—review and editing, S.L. and J.F.W.; visualization, S.L.; supervision, J.F.W. All authors have read and agreed to the published version of the manuscript.

Funding: This search is supported by the National Natural Science Fund under the grant number 10577012.

Institutional Review Board Statement: Not applicable.

Informed Consent Statement: Not applicable.

Data Availability Statement: Sample data available on request.

Acknowledgments: This work was supported and developed by the Shanghai Jiao Tong University and Cranfield University.

Conflicts of Interest: The authors declare no conflict of interest.

Abbreviations

BISMC	Backstepping integral sliding mode control
BNTSM	Backstepping nonsingular terminal sliding mode
CLFs	Control Lyapunov functions
CV	Center of volume
EI	Bending stiffness, E means the elastic modulus, I means the area moment of inertia
NTSM	Nonsingular terminal sliding mode
SMC	Sliding-mode control
RBFNN	Radial basis function neural network

Appendix A

The attitude controller designed by using BNTSM control.

Step 1 Backstepping for the variant of z_1 .

Using the standard backstepping procedure, select the positive definite function, V_1 , as

$$V_1 = \frac{1}{2} z_1^T z_1 \quad (\text{A1})$$

To make the derivative function $\partial V_1 / \partial z_1$ a negative definite, a virtual control is defined as

$$\alpha_1 = G_1^{-1} (\dot{x}_{1r} - c_1 z_1), \quad (\text{A2})$$

where $G_1 = J$, J is in Equation (4). Then,

$$\frac{\partial V_1}{\partial z_1} = z_1^T (\dot{x}_1 - \dot{x}_{1r}) = z_1^T (G_1 \alpha_1 - \dot{x}_{1r}) = -z_1^T c_1 z_1 < 0 \quad (\text{A3})$$

However, instead of directly applying this to virtual control α_1 , a new signal, x_{2r}^0 , is defined as

$$x_{2r}^0 = \alpha_1 - \zeta_2, \tag{A4}$$

where ζ_2 will be designed in Step 2. The command signal, x_{2r}^0 , is filtered to produce the reference signal, x_{2r} , and its derivative, \dot{x}_{2r} . It can be implemented to enforce magnitude and rate limits through the command filter (37). By the design of the command filter (37), the signal $(x_{2,r} - x_{2,r}^0)$ is bounded and small.

The effect of filtering on the tracking error z_1 is estimated by the following stable linear filter

$$\dot{\zeta}_1 = -c_1\zeta_1 + G_1(x_{2,r} - x_{2,r}^0) \tag{A5}$$

where $c_1 > 0$. To remove the effect of filtering the stabilizing functions from the tracking error, the compensated tracking error is defined as

$$\tilde{z}_i = z_i - \zeta_i, \quad (i = 1, 2) \tag{A6}$$

Re-selecting the first Lyapunov function V_1 as a quadratic function of the compensated tracking error is

$$V_1 = \frac{1}{2} \tilde{z}_1^T \tilde{z}_1, \tag{A7}$$

whose derivative is

$$\dot{V}_1 = \tilde{z}_1^T \dot{\tilde{z}}_1 = \tilde{z}_1^T (\dot{x}_1 - \dot{x}_{1r} - \dot{\zeta}_1) = \tilde{z}_1^T (G_1 x_2 - \dot{x}_{1r} - (-c_1\zeta_1 + G_1(x_{2r} - x_{2,r}^0))), \tag{A8}$$

Substituting Equations (A2) and (A4) into Equation (A8) yields

$$\dot{V}_1 = \tilde{z}_1^T (G_1(z_2 + \alpha_1 - \zeta_2)) + \tilde{z}_1^T (c_1\zeta_1 - \dot{x}_{1r}) = -\tilde{z}_1^T c_1 \tilde{z}_1 + \tilde{z}_1^T G_1 \tilde{z}_2 \tag{A9}$$

Step 2 The effect of filtering the command signal on the tracking error, z_2 , is estimated by the following stable linear filter:

$$\dot{\zeta}_2 = -c_2\zeta_2 + G_2(u_a - u_a^0), \tag{A10}$$

where $G_2 = \text{diag}(0, \frac{C_{m_y \delta_e}}{I_y + m_{55}}, \frac{C_{m_z \delta_r}}{I_z + m_{66}}) \cdot \bar{q} S L$, $C_{m_y \delta_e}$, and $C_{m_z \delta_r}$ denote the aerodynamic derivative coefficients of elevator and rudder, respectively, and L is the length of the airship. Note that there is no aileron input for the flexible airship, thus $C_{m_x \delta_a} = 0$, that is, the first roll moment term, is $\frac{C_{m_x \delta_a}}{I_x + m_{44}} = 0$.

Now let us construct the second augmented quadratic CLF by the compensated tracking error, fault estimation error, and parameter disturbance estimation error, as

$$V_2 = V_1 + \frac{1}{2} s^T s + \frac{1}{2} \tilde{d}^T \tilde{d} + \frac{1}{2} e_4^T P_e e_4 + \frac{1}{2} \tilde{u}_f^T P_f^{-1} \tilde{u}_f, \tag{A11}$$

where $\tilde{u}_f = \hat{u}_f - u_f$ is the fault estimation error, \hat{u}_f denotes the estimation of the fault input u_f . In addition, P_e and P_f are positive definite weight matrices. Considering Equation (A9) and substituting Equations (35), (45), (A4), (A6) and (A10) into the derivative of V_2 , yields

$$\begin{aligned}
 \dot{V}_2 &= \tilde{z}_1^T \dot{\tilde{z}}_1 + \mathbf{s}^T \dot{\mathbf{s}} + \tilde{\mathbf{d}}^T \dot{\tilde{\mathbf{d}}} - \mathbf{e}_4^T \mathbf{Q}_e \mathbf{e}_4 + \tilde{\mathbf{u}}_f^T \mathbf{P}_f^{-1} \dot{\tilde{\mathbf{u}}}_f \\
 &= -\tilde{z}_1^T c_1 \tilde{z}_1 + \tilde{z}_1^T \mathbf{G}_1 \tilde{z}_2 + \mathbf{s}^T ((-c_1 \tilde{z}_1 + \mathbf{G}_1 \tilde{z}_2)(1 + \alpha_\gamma \lambda \text{diag}(|\tilde{z}_{1,i}|^{\lambda-1})) \\
 &\quad + \frac{1}{\beta} \cdot \frac{p}{q} |\tilde{z}_2|^{(p/q-1)} (\mathbf{f}_2 + \mathbf{G}_2 \mathbf{u}_a^f + \mathbf{I}_2 \mathbf{d} - \dot{x}_{2r} + c_2 \zeta_2 - \mathbf{G}_2 (\mathbf{u}_a^f - \mathbf{u}_a^{f0}))) + \tilde{\mathbf{d}}^T \dot{\tilde{\mathbf{d}}} - \tilde{\boldsymbol{\xi}}^T \mathbf{Q}_\zeta \tilde{\boldsymbol{\xi}} - \tilde{v}_w^T \mathbf{Q}_{v_w} \tilde{v}_w + \tilde{\mathbf{u}}_f^T \mathbf{P}_f^{-1} \dot{\tilde{\mathbf{u}}}_f \quad (\text{A12}) \\
 &= \tilde{z}_1^T (-c_1 \tilde{z}_1 + \mathbf{G}_1 \tilde{z}_2) + (\mathbf{I}_n + \alpha_\gamma \lambda \text{diag}(|\tilde{z}_{1,i}|^{\lambda-1})) (\mathbf{s}^T \mathbf{G}_1 \tilde{z}_2 - c_1 \tilde{z}_1^T \mathbf{s}) \\
 &\quad + \mathbf{s}^T \frac{1}{\beta} \cdot \frac{p}{q} |\tilde{z}_2|^{(p/q-1)} (\mathbf{f}_2 + \mathbf{I}_2 \mathbf{d} - \dot{x}_{2r} + c_2 \zeta_2 + \mathbf{G}_2 \mathbf{u}_a^{f0}) + \tilde{\mathbf{d}}^T \dot{\tilde{\mathbf{d}}} - \tilde{\boldsymbol{\xi}}^T \mathbf{Q}_\zeta \tilde{\boldsymbol{\xi}} - \tilde{v}_w^T \mathbf{Q}_{v_w} \tilde{v}_w + \tilde{\mathbf{u}}_f^T \mathbf{P}_f^{-1} \dot{\tilde{\mathbf{u}}}_f,
 \end{aligned}$$

where $\tilde{\boldsymbol{\xi}} = \boldsymbol{\xi} - \hat{\boldsymbol{\xi}}, \tilde{v}_w = v_w - \hat{v}_w, \mathbf{u}_a^{f0} = \mathbf{u}_h^0 + \mathbf{u}_f^0$. According to Equation (11), $\mathbf{f}_2 = \frac{1}{M_{22}} (\mathbf{M}_I + \mathbf{M}_G + \mathbf{M}_{AS} + \mathbf{M}_{AD})$; \mathbf{I}_2 denotes elements of the matrix $\mathbf{\Gamma}$ from the 4th row to the 6th one, and

$$\mathbf{M}_{22} = \begin{bmatrix} m_{44} + I_x & 0 & 0 \\ 0 & m_{55} + I_y & 0 \\ 0 & 0 & m_{66} + I_z \end{bmatrix}$$

As \mathbf{d} is an unknown constant or a slow-varying disturbance, then $\dot{\tilde{\mathbf{d}}} = \dot{\hat{\mathbf{d}}} - \dot{\mathbf{d}} \approx \dot{\hat{\mathbf{d}}}$. If \mathbf{d} is a fast-varying process, a RBF-neural network-based backstepping control can be used [33]. The stabilizing function is defined as

$$\mathbf{u}_a^{f0} = \frac{1}{G_2} \left(-\beta \cdot \frac{q}{p} (\mathbf{I}_n + \alpha_\gamma \lambda \text{diag}(|\tilde{z}_{1,i}|^{\lambda-1})) \mathbf{G}_1 |\tilde{z}_2|^{(2-p/q)} - \mathbf{f}_2 - \mathbf{G}_2 \hat{\mathbf{u}}_f - c_2 \tilde{z}_2 + \dot{x}_{2r} - \mathbf{I}_2 \dot{\hat{\mathbf{d}}} - (h\mathbf{s} + \zeta \text{sgn}(\mathbf{s})) \right) \quad (\text{A13})$$

where $c_2 > 0, h, \zeta$ are sliding-mode surface parameters with $h > 0, \zeta > 0$. The control input of \mathbf{u}_h is generated by using the above Equation (A13), and then

$$\begin{aligned}
 \dot{V}_2 &= -\tilde{z}_1^T c_1 \tilde{z}_1 + \tilde{z}_1^T \mathbf{G}_1 \tilde{z}_2 - (\mathbf{I}_n + \alpha_\gamma \lambda \text{diag}(|\tilde{z}_{1,i}|^{\lambda-1})) c_1 \tilde{z}_1^T \mathbf{s} + \mathbf{s}^T \frac{1}{\beta} \cdot \frac{p}{q} |\tilde{z}_2|^{(p/q-1)} (\mathbf{I}_2 (\mathbf{d} - \hat{\mathbf{d}}) + \mathbf{G}_2 (\mathbf{u}_f^0 - \hat{\mathbf{u}}_f) - c_2 \tilde{z}_2) \\
 &\quad - h\mathbf{s}^2 - \zeta \left| \mathbf{s} \right| + \tilde{\mathbf{d}}^T \dot{\tilde{\mathbf{d}}} - \tilde{\boldsymbol{\xi}}^T \mathbf{Q}_\zeta \tilde{\boldsymbol{\xi}} - \tilde{v}_w^T \mathbf{Q}_{v_w} \tilde{v}_w + \tilde{\mathbf{u}}_f^T \mathbf{P}_f^{-1} \dot{\tilde{\mathbf{u}}}_f \\
 &= -\tilde{z}_1^T c_1 \tilde{z}_1 + \tilde{z}_1^T \mathbf{G}_1 \tilde{z}_2 - (\mathbf{I}_n + \alpha_\gamma \lambda \text{diag}(|\tilde{z}_{1,i}|^{\lambda-1})) c_1 \tilde{z}_1^T \mathbf{s} - \mathbf{s}^T \frac{1}{\beta} \cdot \frac{p}{q} |\tilde{z}_2|^{(p/q-1)} c_2 \tilde{z}_2 + \mathbf{s}^T \frac{1}{\beta} \cdot \frac{p}{q} |\tilde{z}_2|^{(p/q-1)} \mathbf{G}_2 \tilde{\mathbf{u}}_f \\
 &\quad - \mathbf{s}^T \frac{1}{\beta} \cdot \frac{p}{q} |\tilde{z}_2|^{(p/q-1)} \mathbf{I}_2 \tilde{\mathbf{d}} + \tilde{\mathbf{d}}^T \dot{\tilde{\mathbf{d}}} - h\mathbf{s}^2 - \zeta \left| \mathbf{s} \right| - \tilde{\boldsymbol{\xi}}^T \mathbf{Q}_\zeta \tilde{\boldsymbol{\xi}} - \tilde{v}_w^T \mathbf{Q}_{v_w} \tilde{v}_w + \tilde{\mathbf{u}}_f^T \mathbf{P}_f^{-1} \dot{\tilde{\mathbf{u}}}_f \quad (\text{A14})
 \end{aligned}$$

As

$$\begin{aligned}
 &-\tilde{z}_1^T c_1 \tilde{z}_1 + \tilde{z}_1^T \mathbf{G}_1 \tilde{z}_2 - (\mathbf{I}_n + \alpha_\gamma \lambda \text{diag}(|\tilde{z}_{1,i}|^{\lambda-1})) c_1 \tilde{z}_1^T \mathbf{s} - \mathbf{s}^T \frac{1}{\beta} \cdot \frac{p}{q} |\tilde{z}_2|^{(p/q-1)} c_2 \tilde{z}_2 \\
 &= -\tilde{z}_1^T c_1 \tilde{z}_1 + \tilde{z}_1^T \mathbf{G}_1 \tilde{z}_2 - (\mathbf{I}_n + \alpha_\gamma \lambda \text{diag}(|\tilde{z}_{1,i}|^{\lambda-1})) c_1 \tilde{z}_1^T (\tilde{\mathbf{z}}_1 + \alpha_\gamma \tilde{\mathbf{z}}_1^\lambda + \frac{1}{\beta} \tilde{\mathbf{z}}_2^{p/q}) - (\tilde{\mathbf{z}}_1 + \alpha_\gamma \tilde{\mathbf{z}}_1^\lambda + \frac{1}{\beta} \tilde{\mathbf{z}}_2^{p/q})^T \frac{1}{\beta} \cdot \frac{p}{q} |\tilde{\mathbf{z}}_2|^{(p/q-1)} c_2 \tilde{\mathbf{z}}_2 \\
 &= -\tilde{z}_1^T c_1 \tilde{z}_1 + \tilde{z}_1^T \mathbf{G}_1 \tilde{z}_2 - (\mathbf{I}_n + \alpha_\gamma \lambda \text{diag}(|\tilde{z}_{1,i}|^{\lambda-1})) \tilde{z}_1^T c_1 \tilde{z}_1 - \alpha_\gamma (\mathbf{I}_n + \alpha_\gamma \lambda \text{diag}(|\tilde{z}_{1,i}|^{\lambda-1})) \tilde{z}_1^T c_1 \tilde{\mathbf{z}}_1^\lambda \\
 &\quad - \frac{1}{\beta} (\mathbf{I}_n + \alpha_\gamma \lambda \text{diag}(|\tilde{z}_{1,i}|^{\lambda-1})) c_1 \tilde{z}_1^T \tilde{\mathbf{z}}_2^{p/q} - \frac{1}{\beta} \cdot \frac{p}{q} \text{diag}(|\tilde{\mathbf{z}}_{2,i}|^{(p/q-1)}) \tilde{z}_1^T c_2 \tilde{\mathbf{z}}_2 \\
 &\quad - \frac{1}{\beta} \cdot \frac{p}{q} \text{diag}(|\tilde{\mathbf{z}}_{2,i}|^{(p/q-1)}) \alpha_\gamma (\tilde{\mathbf{z}}_1^\lambda)^T c_2 \tilde{\mathbf{z}}_2 - \frac{1}{\beta^2} \cdot \frac{p}{q} \text{diag}(|\tilde{\mathbf{z}}_{2,i}|^{(p/q-1)}) (\tilde{\mathbf{z}}_2^{p/q})^T c_2 \tilde{\mathbf{z}}_2 \\
 &= \tilde{z}_1^T \mathbf{G}_1 \tilde{z}_2 - (2\mathbf{I}_n + \alpha_\gamma \lambda \text{diag}(|\tilde{z}_{1,i}|^{\lambda-1})) c_1 \tilde{z}_1^T \tilde{\mathbf{z}}_1 - \alpha_\gamma (\mathbf{I}_n + \alpha_\gamma \lambda \text{diag}(|\tilde{z}_{1,i}|^{\lambda-1})) c_1 |\tilde{\mathbf{z}}_1|^{\lambda-1} \tilde{z}_1^T \tilde{\mathbf{z}}_1 \\
 &\quad - \frac{1}{\beta} (\mathbf{I}_n + \alpha_\gamma \lambda \text{diag}(|\tilde{z}_{1,i}|^{\lambda-1})) c_1 |\tilde{\mathbf{z}}_2|^{p/q-1} \tilde{z}_1^T \tilde{\mathbf{z}}_2 - \frac{1}{\beta} \cdot \frac{p}{q} \text{diag}(|\tilde{\mathbf{z}}_{2,i}|^{(p/q-1)}) c_2 \tilde{z}_1^T \tilde{\mathbf{z}}_2 \\
 &\quad - \frac{1}{\beta} \cdot \frac{p}{q} \text{diag}(|\tilde{\mathbf{z}}_{2,i}|^{(p/q-1)}) \alpha_\gamma |\tilde{\mathbf{z}}_1|^{\lambda-1} c_2 \tilde{z}_1^T \tilde{\mathbf{z}}_2 - \frac{1}{\beta^2} \cdot \frac{p}{q} \text{diag}(|\tilde{\mathbf{z}}_{2,i}|^{(p/q-1)}) |\tilde{\mathbf{z}}_2|^{p/q-1} c_2 \tilde{z}_1^T \tilde{\mathbf{z}}_2 \\
 &= \left[- (2\mathbf{I}_n + \alpha_\gamma \lambda \text{diag}(|\tilde{z}_{1,i}|^{\lambda-1})) c_1 - \alpha_\gamma (\mathbf{I}_n + \alpha_\gamma \lambda \text{diag}(|\tilde{z}_{1,i}|^{\lambda-1})) c_1 |\tilde{\mathbf{z}}_1|^{\lambda-1} \right] \tilde{z}_1^T \tilde{\mathbf{z}}_1 \\
 &\quad + \left(-\frac{1}{\beta} (\mathbf{I}_n + \alpha_\gamma \lambda \text{diag}(|\tilde{z}_{1,i}|^{\lambda-1})) c_1 |\tilde{\mathbf{z}}_2|^{p/q-1} - \frac{1}{\beta} \cdot \frac{p}{q} \text{diag}(|\tilde{\mathbf{z}}_{2,i}|^{(p/q-1)}) c_2 - \frac{1}{\beta} \cdot \frac{p}{q} \text{diag}(|\tilde{\mathbf{z}}_{2,i}|^{(p/q-1)}) \alpha_\gamma |\tilde{\mathbf{z}}_1|^{\lambda-1} c_2 \right) \tilde{z}_1^T \tilde{\mathbf{z}}_2 \\
 &\quad + \tilde{z}_1^T \mathbf{G}_1 \tilde{z}_2 - \frac{1}{\beta^2} \cdot \frac{p}{q} \text{diag}(|\tilde{\mathbf{z}}_{2,i}|^{(p/q-1)}) |\tilde{\mathbf{z}}_2|^{p/q-1} c_2 \tilde{z}_1^T \tilde{\mathbf{z}}_2
 \end{aligned} \quad (\text{A15})$$

and define the positive definite matrix

$$Q = \begin{bmatrix} Q_{11} & \frac{1}{\beta}(\mathbf{I}_n + \alpha_\gamma \lambda \text{diag}(|\tilde{z}_{1,i}|^{\lambda-1})) \left| \tilde{z}_2 \right|^{p/q-1} (c_1 + c_2 \cdot \frac{p}{q}) \\ -G_1 & \frac{1}{\beta^2} \cdot \frac{p}{q} \text{diag}(|\tilde{z}_{2,i}|)^{(p/q-1)} \left| \tilde{z}_2 \right|^{p/q-1} c_2 \end{bmatrix} \tag{A16}$$

where $Q_{11} = \left[(2\mathbf{I}_n + \alpha_\gamma \lambda \text{diag}(|\tilde{z}_{1,i}|^{\lambda-1})) c_1 + \alpha_\gamma (\mathbf{I}_n + \alpha_\gamma \lambda \text{diag}(|\tilde{z}_{1,i}|^{\lambda-1})) c_1 |\tilde{z}_1|^{\lambda-1} \right]$, then it yields

$$-\tilde{z}_1^T c_1 \tilde{z}_1 + \tilde{z}_1^T G_1 \tilde{z}_2 - (\mathbf{I}_n + \alpha_\gamma \lambda \text{diag}(|\tilde{z}_{1,i}|^{\lambda-1})) c_1 \tilde{z}_1^T s - s^T \frac{1}{\beta} \cdot \frac{p}{q} \left| \tilde{z}_2 \right|^{(p/q-1)} c_2 \tilde{z}_2 = - \begin{bmatrix} \tilde{z}_1^T & \tilde{z}_2^T \end{bmatrix} Q \begin{bmatrix} \tilde{z}_1 \\ \tilde{z}_2 \end{bmatrix} \tag{A17}$$

Choose the update law as

$$\dot{\hat{d}} = \left(\frac{1}{\beta} \cdot \frac{p}{q} \left| \tilde{z}_2 \right|^{(p/q-1)} F_2 \right)^T s \tag{A18}$$

In addition, the fault estimator is designed as

$$\dot{\hat{u}}_f = P_f \left(\frac{1}{\beta} \cdot \frac{p}{q} \left| \tilde{z}_2 \right|^{(p/q-1)} G_2 \right)^T \tilde{z}_2 - \gamma_f \hat{u}_f \tag{A19}$$

which yields

$$\begin{aligned} \tilde{u}_f^T P_f^{-1} \dot{\hat{u}}_f &= \tilde{u}_f^T P_f^{-1} \left(\dot{\hat{u}}_f - \dot{u}_f \right) \\ &= \tilde{u}_f^T P_f^{-1} P_f \left(\frac{1}{\beta} \cdot \frac{p}{q} \left| \tilde{z}_2 \right|^{(p/q-1)} G_2 \right)^T \tilde{z}_2 - \tilde{u}_f^T P_f^{-1} \gamma_f \hat{u}_f - \tilde{u}_f^T P_f^{-1} \dot{u}_f \\ &= \tilde{u}_f^T \left(\frac{1}{\beta} \cdot \frac{p}{q} \left| \tilde{z}_2 \right|^{(p/q-1)} G_2 \right)^T \tilde{z}_2 - P_f^{-1} \gamma_f \tilde{u}_f^T \hat{u}_f - P_f^{-1} \tilde{u}_f^T \dot{u}_f \end{aligned} \tag{A20}$$

As $\|u_f\| \leq \bar{u}_{\max} < \infty, \|\dot{u}_f\| \leq \bar{\dot{u}}_{\max} < \infty, \bar{u}_{\max}$ and $\bar{\dot{u}}_{\max}$ denote upper bounds of the actuator position and rotation rate, then

$$-P_f^{-1} \gamma_f \tilde{u}_f^T \hat{u}_f = P_f^{-1} \gamma_f \tilde{u}_f^T (\tilde{u}_f + u_f) \leq \frac{1}{2} \left(-P_f^{-1} \gamma_f \tilde{u}_f^T \tilde{u}_f + P_f^{-1} \gamma_f \bar{u}_{\max}^2 \right) \tag{A21}$$

$$-P_f^{-1} \tilde{u}_f^T \dot{u}_f \leq \frac{1}{2} \left(P_f^{-1} \tilde{u}_f^T \tilde{u}_f + P_f^{-1} \bar{\dot{u}}_{\max}^2 \right) \tag{A22}$$

Substitute (A21); (A22) into (A20) yields

$$\tilde{u}_f^T P_f^{-1} \dot{\hat{u}}_f \leq \tilde{u}_f^T \left(\frac{1}{\beta} \cdot \frac{p}{q} \left| \tilde{z}_2 \right|^{(p/q-1)} G_2 \right)^T \tilde{z}_2 + \bar{c} \tag{A23}$$

where

$$\bar{c} = \frac{1}{2} \left(-P_f^{-1} \gamma_f \tilde{u}_f^T \tilde{u}_f + P_f^{-1} \gamma_f \bar{u}_{\max}^2 \right) + \frac{1}{2} \left(P_f^{-1} \tilde{u}_f^T \tilde{u}_f + P_f^{-1} \bar{\dot{u}}_{\max}^2 \right) \tag{A24}$$

Let $Z_{12} = \begin{bmatrix} \tilde{z}_1^T & \tilde{z}_2^T \end{bmatrix}^T$, and thus, it finally yields

$$\begin{aligned} \dot{V}_2 &= -Z_{12}^T Q Z_{12} - h s^2 - \varsigma \left| s \right| - \tilde{\xi}^T Q_{\tilde{\xi}} \tilde{\xi} - \tilde{v}_w^T Q_{v_w} \tilde{v}_w + \bar{c} \\ &\leq -Z_{12}^T Q Z_{12} - h s^2 - \varsigma \left| s \right| - \sum_{i=1}^3 q_{\xi_i} \tilde{\xi}_i^2 - \sum_{i=1}^3 q_{w_i} \tilde{v}_{w_i}^2 + \bar{c} \end{aligned} \tag{A25}$$

where q_{ξ_i} and q_{w_i} are diagonal elements of matrices of $Q_{\tilde{\xi}}$ and Q_{v_w} , respectively. Using (A16), it is obtained that

$$\begin{aligned}
 |Q| &= \left| \begin{bmatrix} Q_{11} & \frac{1}{\beta} (I_n + \alpha_\gamma \lambda \text{diag}(|\tilde{z}_{1,i}|^{\lambda-1})) |\tilde{z}_2|^{p/q-1} (c_1 + c_2 \cdot \frac{p}{q}) \\ -G_1 & \frac{1}{\beta^2} \cdot \frac{p}{q} \text{diag}(|\tilde{z}_{2,i}|)^{(p/q-1)} |\tilde{z}_2|^{p/q-1} c_2 \end{bmatrix} \right| \\
 &= \left[(2I_n + \alpha_\gamma \lambda \text{diag}(|\tilde{z}_{1,i}|^{\lambda-1})) c_1 + \alpha_\gamma (I_n + \alpha_\gamma \lambda \text{diag}(|\tilde{z}_{1,i}|^{\lambda-1})) c_1 |\tilde{z}_1|^{\lambda-1} \right] \cdot \left(\frac{1}{\beta^2} \cdot \frac{p}{q} \text{diag}(|\tilde{z}_{2,i}|)^{(p/q-1)} |\tilde{z}_2|^{p/q-1} c_2 \right) \\
 &+ \frac{1}{\beta} (I_n + \alpha_\gamma \lambda \text{diag}(|\tilde{z}_{1,i}|^{\lambda-1})) c_1 |\tilde{z}_2|^{p/q-1} G_1 + \frac{1}{\beta} \cdot \frac{p}{q} \text{diag}(|\tilde{z}_{2,i}|)^{(p/q-1)} c_2 (1 + \alpha_\gamma |\tilde{z}_1|^{\lambda-1}) G_1 \\
 &= \left(\frac{1}{\beta} \cdot \text{diag}(|\tilde{z}_{2,i}|)^{(p/q-1)} \right) \left(\frac{1}{\beta} \cdot \frac{p}{q} c_1 c_2 \left(2I_n + \alpha_\gamma (\lambda + I) |\tilde{z}_1|^{\lambda-1} + \alpha_\gamma^2 \lambda |\tilde{z}_1|^{2\lambda-2} \right) \cdot (|\tilde{z}_2|^{p/q-1}) + (I_n + \alpha_\gamma \lambda |\tilde{z}_1|^{\lambda-1}) (c_1 + c_2 \cdot \frac{p}{q}) G_1 \right)
 \end{aligned} \tag{A26}$$

If the following condition is satisfied,

$$(I_n + \alpha_\gamma \lambda |\tilde{z}_1|^{\lambda-1}) (c_1 + c_2 \cdot \frac{p}{q}) G_1 > -\frac{1}{\beta} \cdot \frac{p}{q} c_1 c_2 \left(2I_n + \alpha_\gamma (\lambda + I) |\tilde{z}_1|^{\lambda-1} + \alpha_\gamma^2 \lambda |\tilde{z}_1|^{2\lambda-2} \right) \cdot (|\tilde{z}_2|^{p/q-1}) \tag{A27}$$

then Q is a positive definite, and if $\varsigma > 0$, then

$$\dot{V}_{2,1} = -z_{12}^T Q z_{12} - \varsigma |s| < 0. \tag{A28}$$

Let $c_k = \min\{2Q, 2\varsigma, -\gamma_f + 1, 2q_{\zeta_i}, 2q_{w_i}\} > 0$ ($i = 1, 2, 3$), then

$$\dot{V}_2 \leq -c_k V_2 + \bar{c}. \tag{A29}$$

According to LaSalle-Yoshizawa Lemma [34] and referring to [32], the closed-loop system tracking error will exponentially converge, and

$$V_2 \leq (V_2(0) - \bar{c}/c_k) e^{-c_k t} + \bar{c}/c_k \tag{A30}$$

Hence

$$\frac{1}{2} \tilde{z}_i^T \tilde{z}_i \leq V_2, \|\tilde{z}_i\| \leq \sqrt{\frac{2\bar{c}}{c_k}} \tag{A31}$$

that is, the desired tracking error will exponentially converge to the set $\|\tilde{z}_i\| \leq \sqrt{\frac{2\bar{c}}{c_k}}$, and

$$\|x_1\| = \|\tilde{z}_1 + \zeta_1\| \leq \|\tilde{z}_1\| + \|\zeta_1\|, \|x_2\| = \|\tilde{z}_2 + \zeta_2\| \leq \|\tilde{z}_2\| + \|\zeta_2\| \tag{A32}$$

References

1. Khoury, G.A.; Gillett, J.D. *Airship Technology*, 2nd ed.; Cambridge University Press: Cambridge, UK, 2018; pp. 431–519.
2. Alexandra, M.; Azinheira, J.R.; Paiva, E.D.; Bueno, S.S. Airship Robust Path-tracking: A Tutorial on Airship Modeling and Gain-scheduling Control Design. *Contr. Eng. Pract.* **2016**, *50*, 22–36.
3. Liu, S.Q.; Sang, Y.G. Underactuated Stratospheric Airship Trajectory Control Using an Adaptive Integral Backstepping Approach. *J. Aircr.* **2018**, *55*, 2357–2371. [\[CrossRef\]](#)
4. Liu, S.Q.; Sang, Y.J.; Whidborne, J.F. Adaptive sliding-mode-backstepping trajectory tracking control of underactuated airships. *Aerosp. Sci. Technol.* **2020**, *97*, 105610. [\[CrossRef\]](#)
5. Liu, C.; Wei, Y.; Wang, Y. Finite-time Trajectory Tracking Control for Autonomous Airships with Uncertainties and External Disturbances. *IET Intell. Trans. Syst.* **2020**, *14*, 440–448.
6. Amir, S.; Liu, Y.; Shah, Z.M.; Wang, L.; Zuo, Z.Y.; Wang, Q.G. Higher Order Sliding Mode based Lateral Guidance and Control of Fless Airship. *Aerosp. Sci. Technol.* **2021**, *113*, 106670. [\[CrossRef\]](#)
7. Yuan, J.; Zhu, M.; Guo, X.; Lou, W.J. Finite-time Trajectory Tracking Control for a Stratospheric Airship with Full-state Constraint and Disturbances. *J. Frankl. Inst.* **2021**, *358*, 1499–1528. [\[CrossRef\]](#)
8. Liu, S.Q.; Whidborne, J.F. Neural Network Adaptive Backstepping Fault Tolerant Control for Unmanned Airships with Multi-vector Thrusters. *Proc. Inst. Mech. Eng. Part G J. Aerosp. Eng.* **2021**, *235*, 1507–1520. [\[CrossRef\]](#)
9. Hou, W.; Zhou, P.; Wang, Y.; Wang, N.; Duan, D.P. Station-keeping Control of an Underactuated Stratospheric Airship. *Int. J. Fuzzy Syst.* **2019**, *21*, 715–732.
10. Krstic, M.; Kanellakopoulo, S.I.; Kokotovic, P. *Nonlinear and Adaptive Control Design*; John Wiley & Sons, Inc.: Hoboken, NJ, USA, 1995; pp. 22–66.

11. Liu, S.Q.; Whidborne, J.F. Observer-based Incremental Backstepping Sliding Mode Fault-tolerant Control for Blended-wing-body Aircrafts. *Neurocomputing* **2021**, *464*, 546–561. [[CrossRef](#)]
12. Liu, S.; Liu, Y.; Wang, N. Nonlinear Disturbance Observer-based Backstepping Finite-time Sliding Mode Tracking Control of Underwater Vehicles with System Uncertainties and External Disturbances. *Nonlinear Dyn.* **2017**, *88*, 465–476. [[CrossRef](#)]
13. Yang, Y.N. A Time-specified Nonsingular Terminal Sliding Mode Control Approach for Trajectory Tracking of Robotic Airships. *Nonlinear Dyn.* **2018**, *92*, 1359–1367. [[CrossRef](#)]
14. Mofid, O.; Mobayen, S.; Zhang, C.W.; Esakki, B. Desired Tracking of Delayed Quadrotor UAV under Model Uncertainty and Wind Disturbance using Adaptive Super-twisting Terminal Sliding Mode Control. *ISA Trans.* **2021**, 1–17, *in press*. [[CrossRef](#)]
15. Alattas, K.A.; Mofid, O.; Alanazi, A.K.; Abo-Dief, H.M.; Bartoszewicz, A.; Bakouri, M.; Mobayen, S. Barrier Function Adaptive Nonsingular Terminal Sliding Mode Control Approach for Quad-Rotor Unmanned Aerial Vehicles. *Sensors* **2022**, *22*, 909. [[CrossRef](#)]
16. Pouzesh, M.; Mobayen, S. Event-triggered Fractional-order Sliding Mode Control Technique for Stabilization of Disturbed Quadrotor Unmanned Aerial Vehicles. *Aerosp. Sci. Technol.* **2022**, *121*, 107337. [[CrossRef](#)]
17. Vieira, H.S.; Paiva, E.C.D.; Moriguchi, S.K.; Carvalho, J.R.H. Unified Backstepping Sliding Mode Framework for Airship Control Design. *IEEE Trans. Aerosp. Electr. Syst.* **2020**, *56*, 3246–3258. [[CrossRef](#)]
18. Liu, S.Q.; Whidborne, J.F.; He, L. Backstepping Sliding-mode Control of Stratospheric Airships using Disturbance-observer. *Adv. Space Res.* **2021**, *67*, 1174–1187. [[CrossRef](#)]
19. Guo, X.G.; Xu, W.D.; Wang, J.L.; Park, J.H. Distributed Neuroadaptive Fault-tolerant Sliding-mode Control for 2-D Plane Vehicular Platoon Systems with Spacing Constraints and Unknown Direction Faults. *Automatica* **2021**, *129*, 109675. [[CrossRef](#)]
20. Xiao, C.; Han, D.; Wang, Y.; Zhou, P.F.; Duan, D.P. Fault-tolerant Tracking Control for a Multi-vector Thrust Ellipsoidal Airship using Adaptive Integral Sliding Mode Approach. *Proc. IMechE Part G J. Aerosp. Eng.* **2018**, *232*, 1911–1924. [[CrossRef](#)]
21. Li, Y.W.; Nahon, M.; Sharf, I. Dynamics Modeling and Simulation of Flexible Airships. *AIAA J.* **2009**, *47*, 592–605. [[CrossRef](#)]
22. Li, Y.W.; Nahon, M.; Sharf, I. Airship Dynamics Modeling: A Literature Review. *Progr. Aerosp. Sci.* **2011**, *47*, 217–239. [[CrossRef](#)]
23. Bennaceur, S.; Azouz, N.; Abichou, A. An Efficient Modelling of Flexible Blimps: Eulerian Approach. In Proceedings of the ASME 2007 International Design Engineering Technical Conferences & Computers and Information in Engineering Conference, IDETC/CIE 2007, Las Vegas, NV, USA, 4–7 September 2007; pp. 1–10.
24. Bennaceur, S.; Azouz, N. Contribution of the Added Masses in the Dynamic Modeling of Flexible Airships. *Nonlinear Dyn.* **2012**, *67*, 215–226. [[CrossRef](#)]
25. Han, D.; Yan, L.; Yan, G.Z.; Wang, X.L.; Duan, D.P. Integral Command Filtered Backstepping Control of a Flexible UAV. In Proceedings of the International Conference on Electrical Engineering, Control and Robotics, Chengdu, China, 12–14 January 2018; pp. 1–7.
26. Zhang, Y.M.; Jiang, J. Integrated Design of Reconfigurable Fault Tolerant Control Systems. *J. Guid. Contr. Dyn.* **2001**, *24*, 133–136. [[CrossRef](#)]
27. Tao, G.; Ma, X.; Joshi, S. Adaptive State Feedback and Tracking Control of Systems with Actuator Failures. *IEEE Trans. Autom. Contr.* **2001**, *46*, 78–95. [[CrossRef](#)]
28. Zheng, Z.W.; Zhu, M.; Shi, D.L.; Wu, Z. Hovering Control for a Stratospheric Airship in Unknown Wind. In Proceedings of the AIAA Guidance, Navigation, and Control Conference, AIAA SciTech Forum, National Harbor, MD, USA, 13–17 January 2014; pp. 1–16.
29. Van, M.; Mavrovouniotis, M.; Ge, S.S. An Adaptive Backstepping Nonsingular Fast Terminal Sliding Mode Control for Robust Fault Tolerant Control of Robot Manipulators. *IEEE Trans. Syst. Man Cybern. Part B Cybern.* **2019**, *49*, 1448–1458. [[CrossRef](#)]
30. Chen, S.Y.; Lin, F.J. Robust Nonsingular Terminal Sliding Mode Control for Nonlinear Magnetic Bearing System. *IEEE Trans. Control Syst. Technol.* **2011**, *19*, 636–643. [[CrossRef](#)]
31. Chen, W.H.; Yang, J.; Guo, L.; Li, S.H. Disturbance-Observer-Based Control and Related Methods—an overview. *IEEE Trans. Ind. Electron.* **2016**, *63*, 1083–1095. [[CrossRef](#)]
32. Jin, X. Adaptive Fault Tolerant Control for a Class of Input and State Constrained MIMO Nonlinear Systems. *Int. J. Robust Nonlinear Control* **2016**, *26*, 286–302. [[CrossRef](#)]
33. Liu, S.Q.; Whidborne, J.F.; Chumalee, S. Disturbance Observer Enhanced Neural Network LPV Control for a Blended-wing-body large Aircraft. *IEEE Trans. Aerosp. Electron. Syst.* **2021**, *57*, 2689–2703. [[CrossRef](#)]
34. Khalil, H.K. *Nonlinear Systems*, 3rd ed.; Pearson Education: London, UK, 2002; p. 124.

2022-04-11

Adaptive backstepping nonsingular terminal sliding-mode attitude control of flexible airships with actuator faults

Liu, Shiqian

MDPI

Liu S, Whidborne JF, Song S, Lyu W. (2022) Adaptive backstepping nonsingular terminal sliding-mode attitude control of flexible airships with actuator faults. *Aerospace*, Volume 9, Issue 4, April 2022, Article number 209

<https://doi.org/10.3390/aerospace9040209>

Downloaded from Cranfield Library Services E-Repository